NUCLEAR MAGNETIC RESONANCE IN METALS

By

GEORGE ANDREW MATZKANIN

A DISSERTATION PRESENTED TO THE GRADUATE COUNCIL OF
THE UNIVERSITY OF FLORIDA
IN PARTIAL FULFILLMENT OF THE REQUIREMENTS FOR THE
DEGREE OF DOCTOR OF PHILOSOPHY

UNIVERSITY OF FLORIDA

April, 1966

ACKNOWLEDGMENTS

The author wishes to acknowledge and thank the persons named below for their contributions in bringing the work described in this dissertation to a successful completion.

The author's Ph.D. committee was composed of Drs. T. A. Scott, A. A. Broyles, T. L. Bailey, F. E. Dunnam, and R. G. Blake. Special thanks are due committee chairman and research supervisor Dr. T. A. Scott under whose guidance this research was undertaken.

Dr. Richard Fearn and Mr. Basil McDowell are responsible for the construction of the high-pressure generating system used in these experiments. The author is especially indebted to Mr. McDowell for his assistance in maintaining the pressure system and his help in keeping it operating properly. Mr. Ed Milton supervised construction of the high-pressure bomb which was machined in the Physics Shop of the University of Florida.

A special note of gratitude is due Dr. Ralph Brooker who assisted in the design and construction of the rf spectrometer, and who helped the experiment get off the ground by taking part in the initial studies of the Knight shift in lead. The additional help and counsel of colleagues Mr. Paul Canepa, Mr. Aime DeReggi, Mr. Bill Cornette and Mr. K. S. Krishnan are also gratefully acknowledged.

The author's wife, Mrs. Mary Kay Matzkanin typed the rough draft of the dissertation and provided encouragement at otherwise frustrating times. Mrs. Margaret Dunn typed the final copy of the manuscript and Mr. Ted Coleman prepared the drawings.

Special appreciation is also extended to the author's parents, Mr. and Mrs. George Matzkanin who did everything possible to afford the author the opportunity for the educational goals which have led to this dissertation.

This work was supported by grants numbers NSF-GP-1866 and NSF-GP-4920 from the National Science Foundation.

TABLE OF CONTENTS

LIST OF FIGURES

CHAPTER I

INTRODUCTION

General Remarks

Since the first successful nuclear magnetic resonance experiments were performed in 1946 by Purcell, Pound, and Torrey at Harvard [1] and by Bloch, Hansen, and Packard at Stanford [2], the technique has become a major tool in the study of the finer properties of bulk matter. New insights into the physics of atoms and molecules in the gaseous, liquid, and solid state have resulted from the application of nuclear resonance. The uses of nuclear resonance have multiplied and the techniques have become more specialized until each application of the tool has become practically a field in itself. Although the fundamental interactions between nuclei and between electrons are the same regardless of the state of the matter involved, these interactions are useful in interpreting specific resonance measurements only when the theory is appropriately specialized with regard to the electronic structure and state of internal motion of the matter. The work presented in this paper will be concerned specifically with the study of nuclear magnetic resonance in metals. The next several paragraphs will set forth the fundamental concepts of nuclear magnetic resonance, and then in the next section the situation will be restricted to the case of metals. The theories discussed qualitatively in this chapter will be treated in more detail in Chapter II.

It is known that the spin of a nucleus gives rise to a magnetic dipole moment $\vec{\mu}$ which will interact with an applied magnetic field $\vec{H}_o$ according to the Hamiltonian

$$\underset{\sim}{H} = -\vec{\mu}\cdot\vec{H}_o = -\gamma\hbar\vec{I}\cdot\vec{H}_o \qquad (1)$$

where γ, called the gyromagnetic ratio, is the ratio between the magnetic moment and the spin angular momentum $\hbar\vec{I}$. With $\vec{H}_o$ along the z-axis, the energy levels are simply

$$E_m = -\gamma\hbar H_o m \qquad (2)$$

where $m = \langle I_z \rangle$ takes on the $2I + 1$ values $-I$, $-I + 1$, ..., 0, ..., $I - 1$, I. One might hope to be able to detect the presence of such a set of energy levels by some form of spectral absorption. Transitions may be induced between these levels by supplying electromagnetic energy at the angular frequency ω_o such that

$$\hbar\omega_o = \Delta E = \gamma\hbar H_o \ . \qquad (3)$$

So we have

$$\omega_o = \gamma H_o \qquad \left(\nu_o = \frac{\gamma}{2\pi} H_o\right) \ . \qquad (4)$$

This corresponds to the Larmor precession frequency of a dipole moment about a magnetic field. The probability for a transition is very weak until the resonant condition $\nu_o = \gamma H_o/2\pi$ is satisfied. The probability for transition then greatly increases and gives rise to the phenomenon of nuclear magnetic resonance (NMR). The frequencies for nuclear magnetic resonance are ordinarily in the radio frequency range — about 10 MHz for fields of 3 to 10 kOe.

In the typical NMR experiment, energy is transferred from a radio frequency circuit to a nuclear spin system immersed in a strong uniform magnetic field. In practice this is a sample of perhaps 1 cm^3 contained in a coil of wire which is between the pole faces of a suitable magnet, the coil being part of the tank circuit of an rf oscillator. The frequency of the oscillator can be varied, and at the frequency $\nu_o = \gamma H_o/2\pi$, nuclear resonance occurs. The spins are loosely coupled to each other and to the lattice so that in the absence of an rf field, the spins are at thermal equilibrium and distributed according to the Boltzmann distribution. There is thus an excess of spins in the lower energy states. Upon application of an rf field of frequency ν_o, both stimulated emission and absorption will occur. Due to the surplus of nuclei in the lower energy states, a net absorption of energy will take place manifesting itself as a change in the Q of the resonating electrical circuit. This is the basis for the detection of the nuclear magnetic resonance signal.

The preceding provides the framework for the occurrence and detection of the phenomenon of nuclear magnetic resonance. In order to obtain useful results from experimental data, several influencing factors need to be considered. The information available from an NMR experiment is contained in the descriptive parameters of the resonance absorption line, namely its position, width, shape, and intensity. These parameters in turn depend upon the electric and magnetic fields of neighboring nuclei and electrons. For example, the dipolar couplings between nuclei affect the width and shape of the resonance, causing the typical bell-shaped absorption curve; the internal electric field gradients can interact with the electric quadrupole moment of the nucleus (for spin ≥ 1 and non-cubic crystal structure), affecting the magnetic resonance in several ways.

The relaxation of the excited nuclear spins to their lower energy states is also an important aspect of magnetic resonance. A steady application of radiation will cause a dwindling of the excess population which existed in the lower states, and thus will tend to equalize the populations. Since the net number of absorptive transitions is directly proportional to the excess population of the lower state, the absorption of power from the radio frequency circuit will dwindle accordingly and the resonance absorption is said to be undergoing saturation. If the radio frequency excitation is now switched off, the spin system will be found to regain its equilibrium energy distribution gradually. The rate at which the system exchanges energy with the lattice and resumes thermal equilibrium is characterized by the spin-lattice relaxation time T_1. For metals at room temperature, this time is of the order of 1 to 10 milliseconds. One can also consider a spin-spin relaxation time T_2 which characterizes the interaction of the spins among themselves. The spins can be thought of as passing their orientation from one to another through the interacting influence of their individual dipole fields. The lifetime of excited spins may thus be limited by this process.

The general subject of nuclear resonance and the many important influencing factors are treated quite completely in references [3], [4], [5], and [6].

Nuclear Magnetic Resonance in Metals

The Knight shift

Although rather simple in form and concept, the ideas presented in the preceding section have several implications worthy of emphasis.

Clearly the resonance frequency depends explicitly upon the magnetic field at the site of the resonating nucleus, and ordinarily this is not the same as the applied field. Mention has already been made of the fact that couplings between neighboring dipoles affect the width of the resonance. This is due to a spread in the local fields which are set up by the individual nuclear dipole moments. One might reasonably expect the electrons to also have some influence on the local fields, and this is indeed the case.

The magnetic coupling of the electrons to the nucleus arises from the magnetic fields originating either from the motion of the electrical charges or from the magnetic moment associated with the electron spin. In a free atom, the orbital motion of an electron results in magnetic fields on the order of several hundred kOe. Such enormous fields would of course completely dominate the laboratory field H_o. In bulk matter, however, the crystalline electric fields leave the ground state of the orbital angular momentum non-degenerate, causing the expectation values of all components of the orbital angular momentum to vanish. This is called "quenching" of the orbital angular momentum. The orbital motion can nevertheless still contribute a local field at the nucleus. This comes about because the application of a magnetic field will cause a Larmor precession of the electron orbits, thus producing a local field at the nucleus. The applied field also polarizes the electronic shells, producing an additional local field at the nucleus. The shifts in the NMR frequency due to the local fields of the orbital motion of the electrons are called "chemical shifts."

In a metal the electrons often can be unambiguously separated into two distinct groups — the core electrons, and the conduction electrons.

The core electrons nominally consist of electrons with spins paired off in spherically-symmetrical closed shells. Such electrons are not expected to make a contribution to the field at the nucleus. The valence electrons are distributed throughout the metal in spin-up and spin-down Bloch states, and electrons occupy these states in accordance with Fermi-Dirac statistics. In the absence of an external field, there is no preferential orientation for the electron spins, and thus there is zero average magnetic coupling to the nuclei. However, the application of a static field H_o polarizes the electron spins giving rise to a non-vanishing coupling, which sets up a local field at the nucleus. The shift in the NMR frequency due to this paramagnetism of the conduction electrons was first observed by W. Knight in 1949, and is called the Knight shift [7].

Ideally, the measurement should be made on the metal with all of its conduction electron spins paired, and again on the metal as it actually is when in a magnetic field. The former condition is not easily possible in practice (although it has recently been achieved for lithium by saturating the electron spin system [8]) and is usually approximated by a judiciously chosen non-metallic chemical compound. An uncertainty in the true Knight shift arises because of differences in the positions of the resonances in the various possible reference compounds due to the chemical shifts described previously. The chemical shifts are usually an order of magnitude or so less than the Knight shifts, but they nevertheless limit the accuracy to which the Knight shift can be determined by experiment.

In the basic Knight shift experiment, two resonances are observed successively at a fixed rf frequency ν_o – first that of the metal, then that of some non-metallic reference compound (usually an aqueous solution

of a salt of the metal). In the metal, the field the nucleus sees is the sum of the applied field H_o and the added local field ΔH due to the conduction electrons. Thus if an external field H_m allows the resonance condition to be satisfied for a metal, it will be found that another field strength H_r (higher than H_m because of the absence of ΔH in the reference) is necessary to satisfy it in the reference. The difference in fields $H_r - H_m$ is essentially a measure of the added internal field ΔH in the metal. This difference is found to be proportional to the applied field so the Knight shift is defined by the ratio $K = \frac{H_r - H_m}{H_r}$. Alternatively, one may measure the change in frequency in a fixed magnetic field (the metal resonance is at a higher frequency because of the additional local field ΔH). The two descriptions are of course equivalent (however, see [9] for consideration of the chemical shift).

Theoretical justification for the Knight shift was promptly given in 1950 by Townes, Herring, and Knight [10]. Several aspects of the experimental observations pointed to an enhancement of the field in the vicinity of the nucleus due to the strong hyperfine interaction between the nuclear magnetic moments and the conduction electrons in s-states. This interaction was known to cause the hyperfine structure common in optical spectra, and was particularly strong for unpaired s-electrons. It was thus reasoned that if one estimated the unpaired electron spin density at the nucleus in the metal and multiplied the ordinary expression for the hyperfine interaction by it, the result would approximate the additional energy of each nucleus in the field. This point of view leads directly to the expression

$$K = \frac{8\pi}{3} \chi_p \Omega \langle |\psi(0)|^2 \rangle_F \qquad (5)$$

where χ_p is the electron spin paramagnetic susceptibility in cgs volume units, Ω is the atomic volume, and $\psi(0)$ is the value at the nucleus of the wave function normalized over Ω for an electron of the Fermi energy E_F. The average of the square of the function $\psi(0)$ is taken for all electronic states on the Fermi surface. $\langle|\psi(0)|^2\rangle_F$, generally abbreviated P_F, is thus the average probability density at the nucleus for all electronic states on the Fermi surface. A more detailed derivation of K will be given in the next chapter.

The above formula has all of the properties needed to explain the basic experimental results. Several independent calculations of χ_p and P_F have been made giving good agreement with the experimental values of K. The Knight shift formula can be directly compared to experiment only by independently measuring K, P_F, and χ_p. The only case for which all three quantities are known is for lithium metal, and here the agreement with theory is excellent. For a more detailed analysis of the Knight shift and NMR in metals in general see references [4, Ch. 4], [11], and [12].

Modifications of the basic formalism

The basic Knight shift formalism given on the preceding pages appears to correctly describe the situation in the simpler metals. However for metals possessing a more complex band structure (for example, transition metals), it is necessary to modify the basic theory.

It has been mentioned that the core electrons in a metal are not expected to contribute to the local field at the nucleus. It has, however, been shown by Cohen, Goodings, and Heine [13] that the core may make a contribution through the effect of core polarization. Heretofore,

it has been explicitly assumed that the core electrons are distributed in orbitals in which the spins are exactly paired off; that is, for each electron in a spin-up state there is another in an identical spin-down state. This assumption will be correct if there are equal numbers of spin-up and spin-down electrons in the system under consideration. However, in materials with a net spin this is not the case. The existence of a net spin in the system means that a spin-up electron (in our case a spin-up core electron) will see a different exchange potential than will a spin-down electron. The result is that spin-up and spin-down core electrons will have slightly different orbitals, and in particular, the spin-up and spin-down probability densities at the nucleus will not be identical. Thus, the core electrons are polarized by the exchange interaction with the magnetic electrons, and contribute to the total unpaired spin density at the nucleus. In most cases, the core electrons undergo exchange polarization only with the weak paramagnetism of the s-conduction electrons, and the result is a small addition to the direct conduction electron hyperfine interaction. However in the case of unfilled inner shells (such as for transition metals), the effect may be large.

Another modification of the basic Knight shift must be considered in the case of metals with partly filled non-s bands [14]. As has been previously mentioned, the orbital moment in solids is in general quenched by the crystalline fields. There is, however, the possibility of the quenching being partially lifted by spin-orbit coupling resulting in an orbital contribution to the paramagnetism; this is usually a small effect. It has been shown that there is also a second order effect on the order of β^2/Δ, where Δ is the mean bandwidth (β is the Bohr magneton), which can be comparable to the spin paramagnetism in metals with degenerate bands. Thus

in such metals, the orbital paramagnetism may be an appreciable part of the total paramagnetism.

Anisotropic Knight shift

Several times thus far it has been mentioned that only s-electrons directly contribute to the hyperfine field at the nucleus. This is true only for crystals of cubic symmetry, since here the spin dipolar fields vanish for other than s-electrons. For lower than cubic symmetry, however, the anisotropy in the distribution of the electron charge density may allow electrons of non-s character to contribute to the hyperfine field. This contribution is orientation dependent, depending on the orientation of the crystalline axes with respect to the external magnetic field, and gives rise to an additional shift of the NMR frequency. For an axially symmetric charge distribution, this additional shift is given by

$$K_{anis} = \tfrac{1}{2}\chi_p \Omega (3\cos^2\theta - 1) q_F \qquad (6)$$

where q_F is a measure of the anisotropy in charge distribution, and is related to the conduction electron wave function by

$$q_F = \langle \int \psi^* (3\cos^2 \Theta - 1) r^{-3} \psi dV \rangle_F \ . \qquad (7)$$

The integral is over the unit atomic cell, and the average is over the Fermi surface. The angle θ is the angle between the symmetry axis and the external field direction, and Θ is the angle between the radius vector $\vec{r}$ and the external field direction. The orientations $\theta = 0$ and $\theta = \pi/2$ define the limits of this shift. The total Knight shift is of

course the sum of the isotropic s-part discussed previously and this orientation-dependent part produced by the anisotropy in the charge distribution described by non-s wave functions. Thus we have

$$K = K_{iso} + K_{anis} \tag{8}$$

where K_{iso} is the isotropic Knight shift, and K_{anis} is the anisotropic contribution.

Nuclear magnetic resonance experiments in metals are normally carried out on powders because of skin-depth problems (to be discussed more fully in Chapter III). In such polycrystalline samples, essentially all orientations of the crystalline axes with respect to the magnetic field are represented, and the anisotropic contribution to the frequency shift averages to zero. Although the anisotropic contribution does not contribute to the shift of the magnetic resonance frequency in a powder, it does manifest itself by causing an asymmetry in the resonance line shape. A measure, K_{ax}, of the anisotropic Knight shift can thus be determined by an analysis of this line shape. Here K_{ax} represents a measure of the limits of the orientation-dependent shift K_{anis}, and will be called the "anisotropic Knight shift."

Presentation of Problem

Effects of temperature and pressure

Because theoretical calculations of P_F and χ_P usually depend explicitly on the physical dimensions of the unit atomic cell in a metal, it is possible to calculate their dependence on volume with a minimum of additional effort. It is of great interest to compare the

results of such calculations with measurements of the temperature and volume dependence of the Knight shift. Even if the calculations are not completely successful in predicting χ_p or P_F in an absolute sense, it is satisfying to know whether they are able to predict changes of the correct sign and magnitude for these quantities as a function of the lattice parameter of the metal.

In the early measurements of the temperature dependence of the Knight shift in the alkali metals [15], the attempt was made to explain the results in terms of the volume changes accompanying temperature variation, since the factors entering the Knight shift formula are normally expected to be independent of temperature. The volume expansion upon heating is such an obvious and large effect that it was assumed, reasonably enough, that the entire temperature dependence of the Knight shift could be explained on the basis of the volume changes in χ_p and P_F. The agreement between the results of the experiment analyzed in this way and some theoretical calculations was not very good [11, p. 127]. The disagreement suggested that the Knight shift may depend on temperature independently of volume changes.

It was not until the appearance of work on the pressure dependence of the Knight shift by Benedek and Kushida in 1958 [16] that a clear demonstration of an explicit temperature dependence of the Knight shift could be given. They measured the pressure dependence in the alkali metals, and on comparing the results to those from temperature dependence measurements at constant pressure, found that the Knight shift did explicitly depend on temperature independently of volume changes. In fact, the explicit temperature dependence at constant volume turned out to be

comparable in magnitude to the change in Knight shift brought about by thermal-expansion effects.

An hypothesis based on a modulation of P_F by lattice vibrations was put forth by Benedek and Kushida in order to explain the explicit temperature dependence of the Knight shift. They reasoned that the lattice vibrations should not affect the paramagnetic susceptibility χ_p, since the electron spin relaxation time is on the order of 10^{-6} to 10^{-9} second, whereas the characteristic time of a lattice vibration is 10^{-12} second. Therefore, the electron spin cannot accommodate itself to such fluctuations, and the susceptibility takes on a value determined by the equilibrium lattice spacing. Using this viewpoint, the calculated explicit temperature dependences were in good agreement with the experimental values for the alkali metals.

The Knight shift in lead, platinum, and tin

The ideas set forth in the preceding sections serve to illustrate the importance of Knight shift studies in solid state physics. Its relationship to the conduction-electron charge distribution makes it an important tool for investigating the electronic structure of metals. Very few methods are available for experimentally measuring the conduction-electron probability density. Since the initial pressure-dependence work of Benedek and Kushida on the alkali metals and on copper and aluminum, no pressure work on the Knight shift has appeared in the literature (see [17] and [18] for very recent work of Kushida and Rimai). In the meantime, several modifications of the basic Knight shift formalism have been recognized (core polarization and orbital paramagnetism), and more

temperature dependence studies have been made. Thus, further studies of the effects of pressure on the Knight shift appear to be in order. The work described in this paper presents the results of such experiments on three metals — lead, platinum, and tin — with rather different Knight shift properties.

The temperature dependence of the Knight shift in lead was measured by Feldman in 1959 [19], and the effects of alloying with indium were studied by Snodgrass and Bennett in 1963 [20]. The crystal structure of lead is cubic and there are no unfilled core shells; thus, there is no anisotropic Knight shift and the core-polarization mechanism is not expected to be large. The spin is one-half, so there are no quadrupole interactions.

In their paper on the Knight shift in lead-indium alloys, Snodgrass and Bennett point out that it is necessary to take into account the volume changes which accompany alloying in order to fully analyze the data. The lack of knowledge of the change in Knight shift due to volume changes precludes the possibility of confirming or denying the existence of charge oscillations in the lead-indium alloy system. A study of the pressure dependence of the Knight shift in lead would be helpful in determining to what extent volume changes affect the analysis of the Knight shift in lead alloys.

In regard to the explicit temperature dependence of the Knight shift, it would be of interest to see how large an effect this is in a more complicated polyvalent metal like lead, and also to see if it can be explained in terms of the lattice-vibration hypothesis used by Benedek and Kushida for the alkali metals.

Platinum is a transition metal with one electron missing from the 5d-shell. It has a cubic crystal structure. Thus anisotropy is not present, whereas core polarization by the d-band electrons should be important. The spin is one-half, so there are no quadrupole interactions. The Knight shift in metallic platinum and its temperature dependence were first reported by Rowland in 1958 [21]. The results were a radical departure from the usual Knight shift data, giving a large negative shift of -3.52 per cent with a very large temperature dependence. Negative shifts have also been reported in other transition metals and in some intermetallic compounds, and have been explained in terms of core polarization. A detailed interpretation of the negative Knight shift and its large temperature dependence in platinum was given by Clogston, Jaccarino, and Yafet in 1964 [22]. Platinum then presents an original opportunity to study the effect of volume change on the core-polarization Knight shift mechanism and to determine how much of the large temperature dependence is due to thermal expansion.

Tin undergoes a martensitic type phase transition at 18° C, existing as a semi-conductor called grey tin below this temperature, and as a metal called white tin above this temperature. The Knight shift was first studied by Bloembergen and Rowland in 1953 [23]. No shift was observed in the grey tin phase (the conduction electrons here contribute little or nothing to the magnetic susceptibility); however in white tin, a frequency-shifted, markedly-asymmetric, resonance line was observed. This asymmetric resonance was explained in terms of the anisotropic Knight shift, as previously described. There are no unfilled core shells to contribute a large core-polarization mechanism, and the spin is one-half, ruling out quadrupole interactions.

In 1964 Borsa and Barnes [24] discussed the anisotropic resonance line shape, and pointed out that the anisotropic contribution to the Knight shift could be easily obtained from the powder resonance pattern. Data for tin at different temperatures were also given. An attempt to explain the temperature dependence in terms of thermal expansion was not very successful. Tin, then, presents an interesting case for a pressure study. The effects of volume change on the individual contributions, K_{iso} and K_{ax} can be determined and the individual explicit temperature dependences deduced. Since K_{iso} and K_{ax} depend differently on the conduction-electron wave functions (through P_F and q_F respectively), it would be of interest to compare the results.

CHAPTER II

THEORY

The Knight Shift

Electron-nucleus hyperfine interaction

We consider the form of the magnetic coupling between an electron and a nucleus. As long as the nuclear and electron moments $\vec{\mu}_n$ and $\vec{\mu}_e$ are positioned far enough apart, we expect them to interact according to the usual interaction between a pair of magnetic dipoles with the Hamiltonian

$$\underset{\sim}{H} = \frac{\vec{\mu}_e \cdot \vec{\mu}_n}{r^3} - \frac{3(\vec{\mu}_e \cdot \vec{r})(\vec{\mu}_n \cdot \vec{r})}{r^5} \tag{9}$$

where $\vec{r}$ is the radius vector from the nucleus to the electron. As long as the electronic wave function is a state of non-zero angular momentum, such as p or d, we expect equation (9) to be a good approximation. For s-states, however, the electron wave function is non-zero at the nucleus, and for these close distances, the dipole approximation breaks down [4, p. 85]. The correct interaction in this case was first shown by Fermi in 1930 [25] to be

$$\underset{\sim}{H} = -\frac{8\pi}{3} \vec{\mu}_e \cdot \vec{\mu}_n \delta(\vec{r}) \tag{10}$$

where $\delta(\vec{r})$ is the Dirac delta-function and $\vec{r}$ is the position of the electron relative to the nucleus.

It is convenient to re-express equation (10) in terms of the nuclear and electron spins $\vec{I}$ and $\vec{S}$. The magnetic moments are

$$\vec{\mu}_e = -\gamma_e \hbar \vec{S} \tag{11a}$$

$$\vec{\mu}_n = \gamma_n \hbar \vec{I} \tag{11b}$$

and the Hamiltonian becomes

$$\underset{\sim}{H} = \frac{8\pi}{3} \gamma_e \gamma_n \hbar^2 \vec{I} \cdot \vec{S}\, \delta(\vec{r}) \quad . \tag{12}$$

In a metal, the electrons are non-localized so that a given nucleus experiences a magnetic coupling with many electrons. Therefore, the coupling to the electron spins must be summed over the electron spin orientations of many electrons. The total interaction becomes

$$\underset{\sim}{H}_{en} = \frac{8\pi}{3} \gamma_e \gamma_n \hbar^2 \sum_{j,\ell} \vec{I}_j \cdot \vec{S}_\ell\, \delta(\vec{r}_\ell - \vec{R}_j) \tag{13}$$

where now $\vec{r}_\ell$ is the radius vector to the position of the $\ell^{\underline{\text{th}}}$ electron, and $\vec{R}_j$ that to the position of the $j^{\underline{\text{th}}}$ nucleus.

We now consider a system of nuclear moments and of electrons coupled together by the hyperfine interaction. The relative weakness of the hyperfine coupling enables us to treat it by a perturbation theory in terms of the states of the electrons and the nuclear spins. We shall find that we are able to avoid actually specifying the nuclear states by showing that the effect of the interaction is simply to add an effective magnetic field parallel to the applied field. For the electrons, we will consider them to be weakly interacting and use the usual Bloch functions. This has been shown [26] to have considerable theoretical justification for low energy processes

which do not excite the plasma oscillations caused by the strong long range Coulomb interactions.

For the weakly interacting nucleus-electron system, we write the complete zero order wave function ψ as a product of the wave functions ψ_e and ψ_n of the electrons and nuclei

$$\psi = \psi_e \psi_n \ . \tag{14}$$

From perturbation theory, the energy is then

$$E_{en} = \int \psi^* \underset{\sim}{H}_{en} \psi d\tau_e d\tau_n \tag{15}$$

where $d\tau_e$ and $d\tau_n$ indicate integration over electron and nuclear coordinates (spatial and spin). We shall postpone a specification of the nuclear states and first compute the electronic integral

$$\underset{\sim}{H}'_{en} = \int \psi_e^* \underset{\sim}{H}_{en} \psi_e d\tau_e \tag{16}$$

where we denote the integral by $\underset{\sim}{H}'_{en}$ to emphasize that the nuclear coordinates still appear as operators.

Assuming weakly interacting electrons, we take ψ_e as a simple product of one-electron Bloch functions

$$\psi_{\vec{k}} = u_{\vec{k}}(\vec{r}) e^{i\vec{k}\cdot\vec{r}} \ . \tag{17}$$

We now add a spin coordinate to the Bloch function to obtain the final electron function

$$\psi_{\vec{k}s} = u_{\vec{k}} e^{i\vec{k}\cdot\vec{r}} \psi_s \ . \tag{18}$$

The total wave function for the N-electrons, ψ_e, will then be a product of $\psi_{\vec{k}s}$'s properly antisymmetrized to take account of the Pauli

exclusion principle. This can readily be done in terms of the permutation operator P [27]. We have

$$\psi_e = \frac{1}{\sqrt{N!}} \sum_P (-1)^P P\psi_{\vec{k}s}(1)\psi_{\vec{k}'s'}(2)\psi_{\vec{k}''s''}(3)\ldots\psi_{\vec{k}^{N-1}s^{N-1}}(N) \qquad (19)$$

where $(-1)^P$ means to take a plus or minus sign, depending on whether or not the permutation involves an even or an odd number of interchanges. We compute the contribution to equation (16) from the $j^{\underline{th}}$ nuclear spin, and choose the origin of coordinates at that nuclear site ($\vec{R}_j = 0$). So we have

$$\underset{\sim}{H}'_{enj} = \frac{8\pi}{3} \gamma_e \gamma_n \hbar^2 \vec{I}_j \cdot \int \psi_e^* \Sigma_\ell \vec{S}_\ell \delta(\vec{r}_\ell) \psi_e d\tau_e \ . \qquad (20)$$

This integral can be reduced by a procedure similar to that used in the derivation of the Hartree-Fock equation [28].

Let us consider the integral for one term in the sum over ℓ

$$\int \psi_e^* \vec{S}_\ell \delta(\vec{r}_\ell) \psi_e d\tau_e \ . \qquad (21)$$

The wave function given by equation (19) contains N! terms, each term being a product of N factors. Since $\vec{S}_\ell \delta(\vec{r}_\ell)$ is a one-electron operator, it operates on only one factor in each term. Because of the orthogonality relationship between the $\psi_{\vec{k}s}$'s, the contribution to the integral in (21) will vanish unless all the factors in a term from ψ_e^* are identical (except for complex-conjugate signs) to the factors in a given term from ψ_e; this will be true for only one term in ψ_e^* for each term in ψ_e. A term from ψ_e (or ψ_e^*) is either positive or negative, but the product of identical terms from ψ_e and ψ_e^* is always positive. Using the fact that the $\psi_{\vec{k}s}$'s are normalized, the integral in (21) is reduced to a sum of N! one-particle integrals of the form

$$\int \psi^*_{\vec{k}s}(\ell)\vec{S}_\ell \delta(\vec{r}_\ell)\psi_{\vec{k}s}(\ell)d\tau_{e\ell} \ . \qquad (22)$$

Since the $\psi_{\vec{k}s}$ enter ψ_e symmetrically, we expect the same contribution from each $\psi_{\vec{k}s}$, and may thus write the N! terms making up the integral in (21) as

$$\frac{(N-1)!}{N!} \sum_{\vec{k},s} \int \psi^*_{\vec{k}s}(\ell)\vec{S}_\ell \delta(\vec{r}_\ell)\psi_{\vec{k}s}(\ell)d\tau_{e\ell} \ . \qquad (23)$$

All the $\vec{S}_\ell \delta(\vec{r}_\ell)$ are identical except that they operate on different electron coordinates, ℓ, thus they give identical contributions to equation (20) and we have for the contribution from the N electrons

$$\underset{\sim}{H}'_{enj} = \frac{8\pi}{3}\gamma_e\gamma_n\hbar^2\vec{I}_j \cdot \frac{N(N-1)!}{N!} \sum_{\vec{k},s} \int \psi^*_{\vec{k}s}(1)\vec{S}_1\delta(\vec{r}_1)\psi_{\vec{k}s}(1)d\tau_{e1} \qquad (24)$$

where $N(N-1)!/N! = 1$.

We now assume the electrons are quantized along the z-direction by the external static field H_o. Then, the only contribution to equation (24) comes from the z-component of $\vec{S}_1$. Thus we can write

$$\underset{\sim}{H}'_{enj} = \frac{8\pi}{3}\gamma_e\gamma_n\hbar^2 I_{zj} \sum_{\vec{k},s} |\psi_{\vec{k}s}(0)|^2 m_s p(\vec{k},s) \qquad (25)$$

where $p(\vec{k},s)$ is a factor that is one if $\vec{k},s$ are occupied by an electron and zero otherwise, m_s is the m value of state $\psi_{\vec{k}s}$, and $\psi_{\vec{k}s}(0)$ is the wave function evaluated at the position of nucleus j. If we average this expression over a set of occupations $p(\vec{k},s)$ which are representative of the temperature of the electrons, we can write for the effective interaction with the $j^{\underline{th}}$ nucleus

$$\underset{\sim}{H}'_{enj} = \frac{8\pi}{3}\gamma_e\gamma_n\hbar^2 I_{zj} \sum_{\vec{k},s} |\psi_{\vec{k}s}(0)|^2 m_s f(\vec{k},s) \qquad (26)$$

where $f(\vec{k},s)$ is the Fermi function.

If we now consider a typical term in the sum of equation (26) corresponding to a single value of $\vec{k}$, there are two values of m_s, giving

$$\frac{8\pi}{3}\gamma_n\hbar I_{zj}[\gamma_e\hbar(\tfrac{1}{2})f(\vec{k},\tfrac{1}{2})+\gamma_e\hbar(-\tfrac{1}{2})f(\vec{k},-\tfrac{1}{2})]|\psi_{\vec{k}}(0)|^2 \quad . \tag{27}$$

As can be seen, the quantity in the bracket is (apart from a minus sign, since $\vec{\mu}_e = -\gamma_e\hbar\vec{S}$) the average contribution of state $\vec{k}$ to the z-component of electron magnetization of the sample. We shall denote it by $\overline{\mu_{z\vec{k}}}$. In terms of the spin susceptibility of the $\vec{k}^{\text{th}}$ state we have

$$\overline{\mu_{z\vec{k}}} = \chi^s_{\vec{k}} H_o \quad . \tag{28}$$

The total spin susceptibility of the electrons would be

$$\chi^s_e = \sum_{\vec{k}} \chi^s_{\vec{k}} \quad . \tag{29}$$

Thus, equation (27) can be written as

$$-\frac{8\pi}{3}\gamma_n\hbar I_{zj}|\psi_{\vec{k}}(0)|^2\chi^s_{\vec{k}} H_o \tag{30}$$

and the total effective interaction for spin j is

$$H'_{enj} = -\frac{8\pi}{3}\gamma_n\hbar I_{zj}\Big[\sum_{\vec{k}}|\psi_{\vec{k}}(0)|^2\chi^s_{\vec{k}}\Big] H_o \quad . \tag{31}$$

The problem now is to evaluate the summation in the bracket in equation (31). This is done by considering the constant energy surfaces in $\vec{k}$-space. The function $|\psi_{\vec{k}}(0)|^2\chi^s_{\vec{k}}$ is assumed to vary slowly as one moves from one allowed $\vec{k}$ value to the next, so that we can define a density function to describe the number of allowed $\vec{k}$-values in

any region. Let us define $g(E_{\vec{k}},A)dE_{\vec{k}}dA$ as the number of allowed $\vec{k}$-values lying within a volume element $dE_{\vec{k}}dA$ in $\vec{k}$-space between constant energy surfaces $E_{\vec{k}}$ and $E_{\vec{k}} + dE_{\vec{k}}$, where dA is an element of surface area of the constant energy surface. This density function can now be used to convert the summation in equation (31) to an integral

$$\sum_{\vec{k}} |\psi_{\vec{k}}(0)|^2 \chi^s_{\vec{k}} = \int |\psi_{\vec{k}}(0)|^2 \chi^s_{\vec{k}} g(E_{\vec{k}},A)dE_{\vec{k}}dA \ . \tag{32}$$

Now $\chi^s_{\vec{k}}$ depends on the Fermi functions $f(\vec{k},\frac{1}{2})$ and $f(\vec{k},-\frac{1}{2})$ and is thus essentially a function only of the energy $E_{\vec{k}}$

$$\chi^s_{\vec{k}} = \chi^s(E_{\vec{k}}) \ . \tag{33}$$

Thus, for equation (32) we have

$$\sum_{\vec{k}} |\psi_{\vec{k}}(0)|^2 \chi^s_{\vec{k}} = \int |\psi_{\vec{k}}(0)|^2 \chi^s(E_{\vec{k}}) g(E_{\vec{k}},A)dAdE_{\vec{k}} \ . \tag{34}$$

Now in general if we have any function F of E, its average value over the surface of constant energy $E_{\vec{k}}$ is defined as

$$\langle F(\vec{k})\rangle_{E_{\vec{k}}} \equiv \frac{\int F(\vec{k}) g(E_{\vec{k}},A)dA}{\int g(E_{\vec{k}},A)dA} \ . \tag{35}$$

So the integral over dA in equation (34) can be written

$$\int |\psi_{\vec{k}}(0)|^2 g(E_{\vec{k}},A)dA = \rho(E_{\vec{k}})\langle |\psi_{\vec{k}}(0)|^2\rangle_{E_{\vec{k}}} \tag{36}$$

where

$$\rho(E_{\vec{k}}) = \int g(E_{\vec{k}},A)dA \tag{37}$$

giving for our summation

$$\sum_{\vec{k}} |\psi_{\vec{k}}(0)|^2 \chi^2_{\vec{k}} = \int \langle |\psi_{\vec{k}}(0)|^2 \rangle_{E_{\vec{k}}} \chi^s(E_{\vec{k}}) \rho(E_{\vec{k}}) dE_{\vec{k}} \,. \tag{38}$$

Now consider that $\chi^s(E_{\vec{k}})$ is zero for all values of $E_{\vec{k}}$ that are not rather near to the Fermi energy, since for small values of $E_{\vec{k}}$ the two spin states are 100 per cent populated, whereas for large $E_{\vec{k}}$, neither spin state is occupied. We are therefore justified in assuming $\langle |\psi_{\vec{k}}(0)|^2 \rangle_{E_{\vec{k}}}$ varies sufficiently slowly to be evaluated at the Fermi energy and taken outside the integral

$$\sum_{\vec{k}} |\psi_{\vec{k}}(0)|^2 \chi^s_{\vec{k}} = \langle |\psi_{\vec{k}}(0)|^2 \rangle_{E_F} \int \chi^s(E_{\vec{k}}) \rho(E_{\vec{k}}) dE_{\vec{k}} \,. \tag{39}$$

The integral remaining in equation (39) is essentially the total electron spin susceptibility. This may be seen as follows: converting equation (29) to integral form using the density function gives

$$\chi^s_e = \sum_{\vec{k}} \chi^s_{\vec{k}} = \int \chi^s_{\vec{k}} g(E_{\vec{k}}, A) dE_{\vec{k}} dA \tag{40a}$$

$$= \int \chi^s(E_{\vec{k}}) g(E_{\vec{k}}, A) dE_{\vec{k}} dA \tag{40b}$$

which, after performing the integral over A becomes

$$\chi^s_e = \int \chi^s(E_{\vec{k}}) \rho(E_{\vec{k}}) dE_{\vec{k}} \tag{41}$$

and this is exactly the integral appearing in equation (39). Thus we have

$$\sum_{\vec{k}} |\psi_{\vec{k}}(0)|^2 \chi^s_{\vec{k}} = \langle |\psi_{\vec{k}}(0)|^2 \rangle_{E_F} \chi^s_e \,. \tag{42}$$

The total interaction, then, with the $j^{\underline{th}}$ nuclear spin can be written from equations (31) and (42) as

$$\underset{\sim}{H}'_{enj} = - \frac{8\pi}{3} \gamma_n \hbar I_{zj} \langle |\psi_{\vec{k}}(0)|^2 \rangle_{E_F} \chi_e^s H_o \ . \qquad (43)$$

Rearranging terms gives

$$\underset{\sim}{H}'_{enj} = - \gamma_n \hbar I_{zj} \left[\frac{8\pi}{3} \langle |\psi_{\vec{k}}(0)|^2 \rangle_{E_F} \chi_e^s H_o \right] . \qquad (44)$$

We see that this is in the exact form for the interaction of a nucleus with a magnetic field ΔH, since the general form of such an interaction is

$$\underset{\sim}{H} = - \vec{\mu} \cdot \Delta \vec{H} = - \gamma_n \hbar I_z \Delta H \ . \qquad (45)$$

Thus the interaction with the conduction electrons is entirely equivalent to the interaction with an extra magnetic field ΔH, which aids the applied field H_o, and is given in magnitude by the equation

$$\frac{\Delta H}{H_o} = \frac{8\pi}{3} \langle |\psi_{\vec{k}}(0)|^2 \rangle_{E_F} \chi_e^s \ . \qquad (46)$$

This, then, is the Knight shift as given in Chapter I. To coincide with the notation in Chapter I, we write the Knight shift as

$$K = \frac{\Delta H}{H_o} = \frac{8\pi}{3} \chi_P \Omega \langle |\psi(0)|^2 \rangle_F \qquad (47)$$

where χ_P is the electronic paramagnetic susceptibility per unit volume, Ω is the atomic volume, and $\langle |\psi(0)|^2 \rangle_F$ (generally abbreviated P_F) is the average probability density at the nucleus for all electronic states on the Fermi surface.

Since $\langle |\psi(0)|^2 \rangle_F$ is quite difficult to calculate from first principles, a common variation of the above equation is a re-expression in terms of $|\psi_A(0)|^2$, the probability density for an s-electron at the nucleus in the free atom. This quantity (generally abbreviated P_A) can be

determined from the measured hyperfine coupling constant in the atom, a(s), by the relation

$$a(s) = \frac{16\pi}{3} \gamma\beta\hbar|\psi_A(0)|^2 \qquad (48)$$

where γ is the gyromagnetic ratio and β is the Bohr magneton. We then have for the Knight shift

$$K = \frac{a(s)}{2\gamma\beta\hbar} \chi_P \Omega \xi \qquad (49)$$

where

$$\xi = \frac{P_F}{P_A} . \qquad (50)$$

Core polarization

As was mentioned in Chapter I, the core-polarization Knight shift mechanism arises from the hyperfine field of the core s-electrons which have undergone exchange polarization with the outer electrons. The theoretical treatment of the situation is the unrestricted Hartree-Fock method [29]. In the usual Hartree-Fock method, the average energy is varied by independently varying only orbitals with distinct n and ℓ (that is, the assumption is made of doubly filled orbitals in closed shells). In the unrestricted method, however, orbitals with the same n and ℓ but different m_s are varied separately. The resulting variational equations for orbitals of different m_s will thus have a different form. In the case of platinum, for example, if we let the majority of 5d-electrons have spin-up, then since exchange acts only between electrons of parallel spin, a core

electron with spin-up experiences a stronger exchange force than the corresponding core electron with spin-down. In the unrestricted Hartree-Fock method, the variational formalism is modified to allow such pairs of electrons to have different radial functions; one can then calculate $\psi_{n\ell\ \mathrm{up}}(\vec{r})$ and $\psi_{n\ell\ \mathrm{down}}(\vec{r})$ for each $n\ell$ pair in a self-consistent manner. In particular, one obtains non-zero values for the probability density

$$\rho_{ns} = |\psi_{ns\ \mathrm{up}}(0)|^2 - |\psi_{ns\ \mathrm{down}}(0)|^2 \tag{51}$$

of the core electrons resulting in a contribution to the hyperfine field. For exchange polarization with paramagnetic electrons, the resulting hyperfine field is negative (that is, opposed to the applied field).

The core-polarization Knight shift can be written in analogy to the direct Knight shift as

$$K_{cp} = \frac{8\pi}{3}\,\Omega\rho_{ns}\chi_{cp} \tag{52}$$

where ρ_{ns} is the non-vanishing core s-electron probability density as mentioned above, and χ_{cp} is the paramagnetism giving rise to the core polarization. In terms of the hyperfine field, we write

$$K_{cp} = \frac{\Omega}{\beta}\,H_{hf}(cp)\chi_{cp} \tag{53}$$

where

$$H_{hf}(cp) = \frac{8\pi}{3}\,\beta\rho_{ns} \tag{54}$$

and β is the Bohr magneton. In similar notation, the ordinary direct Knight shift due to the s-conduction electrons can be written

$$K_s = \frac{\Omega}{\beta} H_{hf}(s)\chi_s \ . \qquad (55)$$

The total Knight shift is then given by the sum

$$K = K_{cp} + K_s \ . \qquad (56)$$

The core-polarization Knight shift mechanism is present to some extent in all metals, although in the simpler metals it is usually due to exchange polarization with the weak paramagnetism of electrons outside closed shells. It is generally found that the core-polarization hyperfine field $H_{hf}(cp)$ is an order of magnitude or so smaller than the conduction electron hyperfine field $H_{hf}(s)$. Thus, in this case, K_{cp} is negligible compared to K_s. In the d-band transition metals, however, the core can undergo exchange polarization with the electrons in the unfilled inner d-band, and we write

$$K_d = \frac{\Omega}{\beta} H_{hf}(d)\chi_d \ . \qquad (57)$$

The Pauli spin susceptibilities are related to the densities of states at the Fermi surface as follows:

$$\chi_s = \beta^2 N_s(E_F) \qquad (58a)$$

$$\chi_d = \beta^2 N_d(E_F) \qquad (58b)$$

where $N_s(E_F)$ and $N_d(E_F)$ are the densities of states at the Fermi level for s- and d-electrons respectively. Because of the narrow d-band in these metals, they have relatively large values of $N_d(E_F)$ compared to $N_s(E_F)$, and therefore the core-polarization mechanism K_d can be comparable to the direct Knight shift K_s.

Thus there are several distinct contributions to the hyperfine interaction in a transition metal; they arise from the interaction of the nuclear moment with (1) the s-conduction electron spin density, (2) the core s-electrons that have been spin-polarized by the d-band electrons, and (3) the orbital paramagnetism of the degenerate d-band electrons, discussed in Chapter I. There is also the possibility of a contribution from the spin dipole moment of the d-electrons, but this vanishes for cubic symmetry. Each of the contributions to the total hyperfine interaction will contribute to the Knight shift in direct proportion to the strength of the individual hyperfine fields and the magnitudes of the corresponding contributions to the susceptibility. Thus we may write

$$K_s = \frac{\Omega}{\beta} H_{hf}(s)\chi_s \tag{59a}$$

$$K_d = \frac{\Omega}{\beta} H_{hf}(d)\chi_d \tag{59b}$$

$$K_{VV} = \frac{\Omega}{\beta} H_{hf}(orb)\chi_{VV} \tag{59c}$$

where $H_{hf}(s)$, $H_{hf}(d)$, and $H_{hf}(orb)$ are the hyperfine fields for the s-contact, d-core polarization, and orbital interactions respectively; and χ_s, χ_d, and χ_{VV} are the corresponding susceptibilities.

Clearly, the relative importance of any particular contribution (K_s, K_d, or K_{VV}) to the total Knight shift, K, will depend in detail on the relative magnitudes of both the hyperfine fields and susceptibilities, and these, of course, will vary from one metal to the next. For any given transition metal it usually is found [30] that:

(a) $H_{hf}(s)$ is an order of magnitude larger than $H_{hf}(d)$ or $H_{hf}(orb)$,

(b) $H_{hf}(s) > H_{hf}(orb) > 0$ whereas $H_{hf}(d) < 0$,

(c) $H_{hf}(orb)$ increases rapidly with increasing atomic number within a given d-shell, much more so than does $H_{hf}(s)$ or $H_{hf}(d)$,

(d) χ_d exceeds χ_s by a factor varying from 5 to 50,

(e) χ_{VV} and χ_d are of the same order of magnitude except when $N_d(E_F) \ll \overline{N_d(E_F)}$, in which case $\chi_{VV} \gg \chi_d$, or when the d-band is almost filled (or empty), in which case $\chi_{VV} \ll \chi_d$.

Thus one may expect Knight shifts that are large or small, positive or negative, depending on the pecularities of the structure of the d-band of any given transition metal.

Anisotropic Knight shift

It was mentioned at the beginning of the direct Knight shift derivation that the usual dipole-dipole Hamiltonian breaks down for s-states which have a non-zero probability at the nucleus. In this case, the Fermi contact interaction is used. One must, however, still consider the possibility of nuclear dipole-electron dipole interaction at a distance for other than s-states. Here the dipole-dipole approximation is expected to be good.

The complete Hamiltonian for the nuclear spin interaction (for spin one-half) with a conduction electron can be written [3, p. 172]

$$\underset{\sim}{H} = \gamma_e\gamma_n\hbar^2\vec{I}\cdot\left[\frac{8\pi}{3}\vec{s}\delta(\vec{r}) - \left(\frac{\vec{s}}{r^3} - \frac{3\vec{r}(\vec{s}\cdot\vec{r})}{r^5}\right) + \frac{\vec{l}}{r^3}\right] \qquad (60)$$

where $\vec{r}$ is the radius vector of the electron with the nucleus at the origin and $\vec{l}$ is the orbital angular momentum of the electron. The first term is the point interaction discussed previously, the second term represents the interaction with non-s electrons, and the third term represents the interaction with the electron orbit, which is negligible for quenched angular momentum. The second term is found to give rise to the orientation dependent contribution to the Knight shift discussed in Chapter I.

Let us consider the second term in equation (60)

$$\underset{\sim}{H}_{en} = -\gamma_e\gamma_n\hbar^2\vec{I}\cdot\left(\frac{\vec{s}}{r^3} - \frac{3\vec{r}(\vec{s}\cdot\vec{r})}{r^5}\right). \qquad (61)$$

If we denote the angle between the magnetic field direction and the radius vector between electron and nucleus by α, the Hamiltonian can be expressed as the sum of several parts [4, p. 47]. In the first order perturbation calculation, we are only interested in elements diagonal in the nuclear and electron spin, and for unlike spins, the dipolar Hamiltonian reduces to one term [4, pp. 47-58]

$$\underset{\sim}{H}_{en} = -\gamma_e\gamma_n\hbar^2 I_z S_z(1-3\cos^2\alpha)r^{-3}. \qquad (62)$$

As in the case of the direct Knight shift derivation, we consider a system of weakly interacting electrons and write the total wave function as $\psi = \psi_e\psi_n$. The interaction energy is

$$E_{en} = \int \psi^* \underset{\sim}{H}_{en}\psi d\tau_e d\tau_n. \qquad (63)$$

As before, considering only the integration over electron coordinates,

we have

$$\underset{\sim}{H}'_{en} = \int \psi_e^* \underset{\sim}{H}_{en} \psi_e \, d\tau_e \ . \qquad (64)$$

In reducing this integral, we use the same procedure used in the case of the derivation of the isotropic Knight shift earlier in this Chapter. The electron wave function ψ_e is treated as an antisymmetrized product of one-electron functions and we consider only the interaction of a one-particle Hamiltonian $\underset{\sim}{H}_{en}(1)$. The result for the total interaction with N electrons – the total interaction is the sum over N electrons of the single-particle interaction represented by equation (62) – is an integral over a one-electron function $\psi_{\vec{k}s}$ and a sum over all states $\vec{k},s$

$$\underset{\sim}{H}'_{en} = -\gamma_e \gamma_n \hbar^2 I_z \sum_{\vec{k},s} m_s p(\vec{k},s) \int \psi^*_{\vec{k},s} (1-3\cos^2\alpha) r^{-3} \psi_{\vec{k},s} \, d\tau \qquad (65)$$

where $p(\vec{k},s)$ is one if $\vec{k},s$ are occupied and zero otherwise.

We see that this is analogous in form to equation (25). Evaluating the summation as in the case of equation (25), we can write for the total interaction of N electrons with a single nucleus

$$\underset{\sim}{H}'_{en} = \gamma_n \hbar I_z \left[\chi_e^s H_o \langle \int \psi^*_{\vec{k}} (1-3\cos^2\alpha) r^{-3} \psi_{\vec{k}} \, d\tau \rangle_{E_F} \right] \qquad (66)$$

where as before, χ_e^s is the spin paramagnetic susceptibility of the conduction electrons. Once again this is the form for the interaction of a nucleus with a magnetic field ΔH, so we can write

$$\frac{\Delta H}{H_o} = -\chi_e^s \langle \int \psi^*_{\vec{k}} (1-3\cos^2\alpha) r^{-3} \psi_{\vec{k}} \, d\tau \rangle_{E_F} \ . \qquad (67)$$

Equation (67) can be expressed in terms of the orientation of H_o with respect to the crystallographic axes by using the spherical-

harmonic addition theorem [31]. In the x, y, z-crystallographic coordinate system, let the field H_o have the polar angles θ, ϕ, and the radius vector have the polar angles Θ, Φ. By the addition theorem, we have for the Legendre polynomial P_ℓ

$$P_\ell(\cos\alpha) = \frac{4\pi}{2\ell+1} \sum_{m=-\ell}^{\ell} (-1)^m Y_\ell^m(\Theta,\Phi) Y_\ell^{-m}(\theta,\phi) \tag{68}$$

where

$$Y_\ell^m(\theta,\phi) = P_\ell^m(\cos\theta)\frac{e^{im\phi}}{\sqrt{2\pi}} \tag{69}$$

is a surface spherical harmonic and the P_ℓ^m is an associated Legendre polynomial. Now

$$P_2(\cos\alpha) = \tfrac{1}{2}(3\cos^2\alpha - 1) \tag{70}$$

so we have

$$\tfrac{1}{2}(3\cos^2\alpha - 1) = \frac{2}{5} \sum_{m=-2}^{2} (-1)^m P_2^m(\cos\Theta) P_2^{-m}(\cos\theta) e^{im(\Phi-\phi)} \ . \tag{71}$$

On substituting equation (71) into the integral in equation (67) and assuming an axially symmetric electron charge distribution, we see that the integral over Φ will give no contribution unless $m = 0$. For this case, the associated Legendre polynomials are given by

$$P_2^o(\cos\theta) = \left(\frac{5}{2}\right)^{\frac{1}{2}} \tfrac{1}{2}(3\cos^2\theta - 1) \ . \tag{72}$$

Thus we get

$$\frac{\Delta H}{H_o} = \tfrac{1}{2}\chi_P \Omega (3\cos^2\theta - 1) q_F \tag{73}$$

where χ_P is the electronic paramagnetic volume susceptibility, Ω is the atomic volume, and

$$q_F = \langle \int \psi^*(3\cos^2\Theta - 1)r^{-3}\psi d\tau \rangle_F \qquad (74)$$

is a measure of the anisotropy in the charge distribution which vanishes for cubic symmetry.

The shift in the NMR frequency represented by equation (73) is called the anisotropic Knight shift. It is, of course, superimposed on the isotropic shift from the hyperfine contact interaction, so in general we have

$$K = K_{iso} + \tfrac{1}{2}\chi_P \Omega(3\cos^2\theta - 1)q_F \ . \qquad (75)$$

The total frequency shift from the non-metallic reference compound depends on the angle θ between the magnetic field and the symmetry axis and varies between the limits

$$\theta = 0: \quad \Delta\nu_{\parallel} = \Delta\nu_{iso} + \chi_P \Omega q_F \qquad (76a)$$

$$\theta = \frac{\pi}{2}: \quad \Delta\nu_{\perp} = \Delta\nu_{iso} - \tfrac{1}{2}\chi_P \Omega q_F \ . \qquad (76b)$$

In a polycrystalline material, the Knight shift averages to K_{iso}, and thus there is no net shift in the line due to this additional interaction. However, since the number of nuclei in a powdered specimen for which the magnetic field makes an angle θ with the crystallographic z-axis is proportional to sin θ [32], the anisotropic shift manifests itself as a distribution over frequencies producing an asymmetric resonance line. This is illustrated in Figure 1. A detailed analysis of the lineshape [25] indicates that, at sufficiently high fields, the furthest points of maximum slope correspond to the limits $\Delta\nu_{\parallel}$ and $\Delta\nu_{\perp}$ of the anisotropic frequency shift.

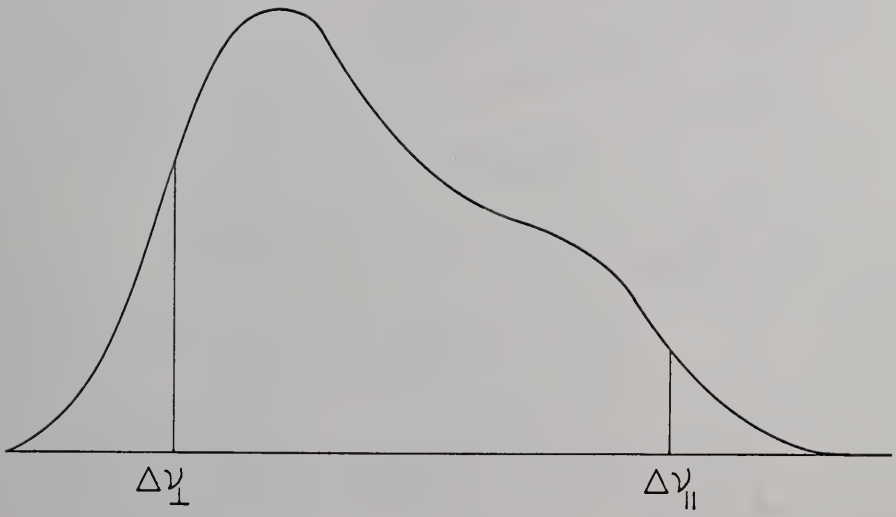

Figure 1. Asymmetric resonance line due to anisotropic Knight shift.

We can define a measure of the anisotropic Knight shift by

$$K_{ax} \equiv \tfrac{1}{2} \chi_P \Omega q_F \ . \tag{77}$$

Then, from equations (76a and 76b) we have

$$\frac{\Delta\nu_{\parallel} - \Delta\nu_{\perp}}{\nu_o} = 3K_{ax} \ . \tag{78}$$

The anisotropic Knight shift is thus deduced from the powder line shape by measuring the distance between the furthest points of maximum slope. The iostropic contribution is measured from a point two-thirds of the way from $\Delta\nu_{\parallel}$ to $\Delta\nu_{\perp}$.

The Effects of Temperature and Pressure

Volume dependence of P_F

As has been pointed out, the basic Knight shift is written

$$K = \frac{8\pi}{3} \chi_P \Omega P_F \tag{79}$$

where $P_F = \langle |\psi(0)|^2 \rangle_F$. A measurement of the pressure dependence of K thus determines the volume dependence of the product $(\chi_P \Omega) P_F$. Clearly, it would be desirable to have an independent measurement of the volume dependence of $\chi_P \Omega$; unfortunately such measurements are not available for lead, platinum, or tin. However, the volume dependence of $\chi_P \Omega$ may be approximated on theoretical grounds.

In the free-electron picture, the Pauli volume susceptibility is given by

$$\chi_P = \beta^2 N(E_F) \tag{80}$$

where $N(E_F)$, the density of states, is

$$N(E_F) = \frac{3n}{2E_F} . \tag{81}$$

Here, n is the electron density and the Fermi energy E_F is given by

$$E_F = \frac{\hbar^2 k_F^2}{2m} \tag{82}$$

where

$$k_F^2 = (3\pi^2 n)^{2/3} . \tag{83}$$

The electron density, n, can be expressed in terms of an effective sphere with radius r_s, where r_s represents the inter-electronic separation. We have

$$\frac{1}{n} = \frac{4}{3} \pi r_s^3 . \tag{84}$$

Combining these equations, we get

$$E_F = \frac{\hbar^2}{2mr_s^2} \left(\frac{9\pi}{4}\right)^{2/3} \tag{85a}$$

$$N(E_F) = \frac{3n}{2} \frac{2mr_s^2}{\hbar^2} \left(\frac{9\pi}{4}\right)^{-2/3} \tag{85b}$$

$$\chi_P = \frac{3nmr_s^2}{\hbar^2} \beta^2 \left(\frac{9\pi}{4}\right)^{-2/3} . \tag{85c}$$

Thus in the free-electron picture, the volume dependence of $\chi_P \Omega$ is simply proportional to $V^{2/3}$.

Another method of calculating $\chi_P \Omega$ is the collective-electron picture of Pines [26] which gives very good agreement with direct experimental evidence in several of the alkali metals. In this theory, Pines takes into account the exchange and correlation

interactions between electrons. The susceptibility is given as

$$\chi_p = \frac{2n\beta^2}{\alpha} \tag{86}$$

where n is the electron density and

$$\alpha = \frac{20}{9} \langle E_F \rangle + \frac{8}{9} E_{exch} + \alpha_{\ell.r.} + \alpha_{s.r.} \cdot \tag{87}$$

Here E_{exch} is the exchange energy, $\langle E_F \rangle$ is the mean Fermi energy per electron, and the last two terms represent the effects of long and short range Coulomb correlations. In Rydbergs per electron, we have

$$E_{exch} = - \frac{0.916}{r_s} \tag{88a}$$

$$\alpha_{\ell.r.} = 0.037 - 0.0432\, r_s^{-\frac{1}{2}} \tag{88b}$$

$$\alpha_{s.r.} = 0.125 - 0.0032\, r_s \cdot \tag{88c}$$

Expressing the Fermi energy in terms of the inter-electronic spacing r_s, as above, we can write

$$\alpha = \frac{4.911}{(\frac{m^*}{m}) r_s^2} - \frac{0.814}{r_s} - \frac{0.0432}{r_s^{\frac{1}{2}}} - 0.0032\, r_s + 0.162 \text{ (Rydberg units)} \tag{89}$$

where m is the mass of the free electron and m^* is the effective mass of the electron in the metal. From equation (86) we then have

$$\chi_p \Omega = \frac{2n\beta^2}{\alpha} \Omega = \frac{.5325 \times 10^{-4}}{\alpha} z \text{ (Bohr units)} \tag{90}$$

where z is the number of conduction electrons per atom. Here, the unit of length is taken as the first Bohr orbit. For a small change in r_s we can write

$$r_s = (r_s)_o (1 + \delta) \tag{91}$$

and thus,

$$\alpha = \alpha_o - \left[\frac{9.82}{(\frac{m^*}{m})(r_s)_o^2} - \frac{.814}{(r_s)_o} - \frac{.0216}{(r_s)_o^{\frac{1}{2}}} + .0032\,(r_s)_o \right] \qquad (92)$$

where

$$\alpha_o = \frac{4.911}{(\frac{m^*}{m})(r_s)_o^2} - \frac{.814}{(r_s)_o} - \frac{.0432}{(r_s)_o^{\frac{1}{2}}} - .0032\,(r_s)_o + .162 \; . \qquad (93)$$

Of course, r_s is related to the volume by

$$\frac{r_s}{(r_s)_o} = (\frac{V}{V_o})^{1/3} \; . \qquad (94)$$

Thus a measurement of the volume dependence of the Knight shift, K, and a calculation of the volume dependence of $\chi_P \Omega$, using either the free-electron picture or the collective-electron picture, enables one to deduce the volume dependence of the probability density P_F.

Explicit temperature dependence

As was mentioned in Chapter I, the observed temperature dependence at constant pressure of the Knight shift is the sum of two contributions: (1) the effect of volume change due to thermal expansion, and (2) the explicit effect of temperature at constant volume. It is possible to separate these two effects by using the thermodynamic relation

$$\left(\frac{\partial w}{\partial x}\right)_y = \left(\frac{\partial w}{\partial z}\right)_x \left(\frac{\partial z}{\partial x}\right)_y + \left(\frac{\partial w}{\partial x}\right)_z \qquad (95)$$

where x, y, z represent the state variables and w is any function of the state of the system. Assuming K to be a function of P, V, and T, and taking $w = \ell n K$, we have

$$\left(\frac{\partial\, \ell n K}{\partial T}\right)_P = \left(\frac{\partial\, \ell n K}{\partial\, \ell n V}\right)_T \left(\frac{\partial\, \ell n V}{\partial T}\right)_P + \left(\frac{\partial\, \ell n K}{\partial T}\right)_V \; . \qquad (96)$$

The left-hand side of this equation represents the observed temperature dependence of K at constant pressure. In the first term on the right-hand side, $\left(\frac{\partial \ell nK}{\partial \ell nV}\right)_T$ is the volume dependence at constant temperature which can be deduced from the pressure dependence at constant temperature by using the compressibility; $\left(\frac{\partial \ell nV}{\partial T}\right)_P$ is, of course, simply the thermal expansion. The second term on the right-hand side represents the explicit temperature dependence at constant volume.

In the discussion on temperature and pressure effects in the first chapter, it was noted that an explicit temperature dependence of K can be explained in terms of the effect of lattice vibrations on P_F. Lattice vibrations are thought of as thermal strain, or rapid changes in the volume occupied by an atom in the lattice. As the lattice vibrates, the electronic wave function at each point in the lattice adjusts itself almost instantaneously to the local state of strain. Thus P_F is a time varying function, which can be expanded around the volume corresponding to the equilibrium volume V_o at temperature T as follows:

$$\overline{P_F(t)} = P_F(V_o) + \left(\frac{\partial P_F}{\partial V}\right)_{V_o} \overline{\Delta V} + \tfrac{1}{2}\left(\frac{\partial^2 P_F}{\partial V^2}\right)_{V_o} \overline{(\Delta V)^2} + \ldots \qquad (97)$$

where the bar indicates a time average and $\Delta V = V(t) - V_o$. The term linear in ΔV vanishes, since $\overline{V(t) - V_o} = 0$. However in second order, $\overline{(\Delta V)^2}$ is always positive and proportional to the squares of the amplitudes of the normal modes of the lattice vibrations. Thus the time average of P_F can be a function of temperature at constant volume through the temperature dependence of the lattice vibrations.

Assuming χ_P to be independent of temperature at constant volume as explained in Chapter I, we can write the logarithmic derivative of

K relative to T at constant volume as

$$\left(\frac{\partial \ell n K}{\partial T}\right)_V = \left(\frac{\partial \ell n \bar{P}_F}{\partial T}\right)_V . \tag{98}$$

From equation (97) we have

$$\left(\frac{\partial \ell n \bar{P}_F}{\partial T}\right)_V = \frac{1}{2P_F(V_o)} \left(\frac{\partial^2 P_F}{\partial (V/V_o)^2}\right)_{V=V_o} \frac{\partial}{\partial T} \overline{\left(\frac{\Delta V}{V_o}\right)^2} . \tag{99}$$

The Debye picture of lattice vibrations can be used to estimate $\overline{\left(\frac{\Delta V}{V_o}\right)^2}$. For temperatures well above the Debye temperature, where the wavelength of the lattice vibrations is of the order of the interatomic distance, we have [16]

$$\overline{\left(\frac{\Delta V}{V_o}\right)^2} \approx \frac{\beta k T}{\Omega} \tag{100}$$

where T is the absolute temperature, k is Boltzmann's constant, β is the volume compressibility, and Ω is the atomic volume. Thus using the experimentally deduced volume dependence of P_F (as explained in the previous section) and equations (98), (99), and (100), it is possible to predict the explicit temperature dependence of K at constant volume.

Recently, Muto, et al. [33] have rigorously derived the effect of lattice vibrations on the Knight shift. They find the Knight shift can be written

$$K = K_o + K_1(T) \tag{101}$$

where

$$K_o = \frac{8\pi}{3} \chi_P \Omega P_F \tag{102}$$

is the Knight shift for a static lattice and $K_1(T)$ is an additional term due to the lattice vibrations, explicitly depending on temperature. The theory is somewhat difficult to apply quantitatively, since a knowledge of the conduction-electron wave functions is needed to evaluate $K_1(T)$. However, the effects of the lattice vibrations are more completely accounted for than in the formalism described on the preceding pages by including the effects on both the conduction-electron probability density and on the hyperfine interacting. Further comparison will be made in Chapter IV in the discussion of the results of the lead experiment.

CHAPTER III

EXPERIMENTAL APPARATUS AND PROCEDURE

The Detection System

General description

A block diagram of the electronics is shown in Figure 2. As was mentioned in Chapter I, the sample under investigation is placed within the coil of the tank circuit of an rf oscillator. The absorption of energy by the resonating nuclei changes the Q of the tank circuit which is manifested as a change in the level of oscillation. In principle, one could simply couple the rf signal to a detector producing a dc voltage proportional to the amplitude of the rf input. The resonance is then exhibited as a small change in the detector's dc output which could be amplified and displayed on a recorder. However, this is only feasible in the case of the strongest resonances, viz. protons.

Usually the changes in the rf level due to electrical noise and accidental variations in the oscillator level are of the same order of magnitude as the change due to resonance. Some method must be provided for distinguishing between these possibilities. This is accomplished by modulating the magnetic field surrounding the sample with an audio frequency. This in essence modulates the absorption process by causing the nuclei to go in and out of resonance, thus

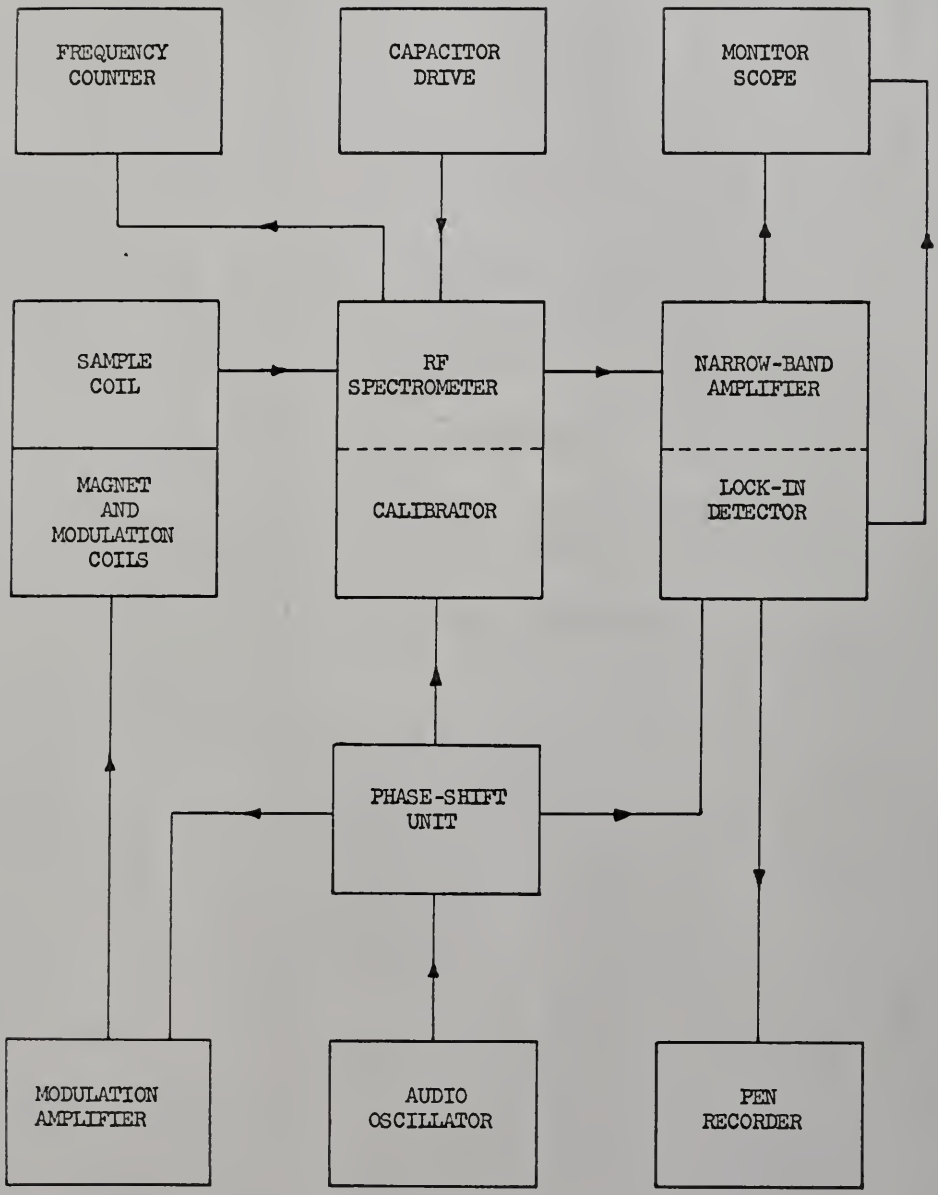

Figure 2. Block diagram of NMR detection system.

producing a corresponding modulation of the rf level. The output of the detector stage is now an ac signal at the modulation frequency with an amplitude proportional to the slope of the absorption curve.

The detected ac signal is fed to a narrow-band amplifier utilizing a twin-tee filter, which provides negative feedback for all frequencies except in a narrow band around the modulation frequency. Thus the resonance signal is amplified, while the noise band width is greatly reduced. The signal now goes to a lock-in detector consisting of a phase-sensitive detector followed by an RC low-pass filter. The output of the phase-sensitive detector is proportional to the phase angle between the input signal and a reference signal of the same frequency. Thus, only signals coherent with the reference are passed. An average voltage $\overline{V}$ is obtained by means of the low-pass filter, which also provides selectivity centered at the reference frequency. Interfering signals close to the reference frequency produce beats in the output which are averaged to zero by the RC filter. The overall effect of noise (which is a random function of time) is to cause fluctuations of $\overline{V}$ about zero. Any desired bandwidth may be obtained by suitably choosing the time constant of the filter.

The dc output of the lock-in detector is fed to a pen recorder which displays the resonance. Since the ac output of the oscillator is determined by the slope of the absorption curve, the signal displayed on the recorder is the derivative of this curve.

The spectrometer

The marginal oscillator [34] has been widely used for NMR experimentation because of its good sensitivity and simplicity; however,

it permits sensitive operation with a good signal-to-noise ratio only in the range of rf levels between .01 and 1 volt. For operation at lower levels, it has been found [35] that incorporating a limiter in the feedback network, along with suitably high rf amplification, permits stable operation. Furthermore, the limiting action discriminates against noise and thus improves the signal-to-noise ratio. Because of the short relaxation times in metals (on the order of milliseconds), it is usually possible to use a rather high level of rf oscillation without undue saturation effects. And, in fact, this is often necessary in order to obtain the optimum signal, since the resonances in metals are generally weak.

The rf oscillator used in these experiments was patterned after a design for a high-level oscillator published by Knight [36]. The basic oscillator circuit is shown in Figure 3. It is essentially a modification of the basic marginal oscillator, possessing some of the advantages of both the marginal and the limiting modes of operation. The basic oscillator-detector consists of only a single vacuum tube (6922) in which are performed regeneration, limiting, and detection. The first section of the twin triode is a cathode follower. The second half operates both as a cathode-driven detector and as a plate-limited rf amplifier. Regenerative coupling from the amplifier plate is provided by a 5 pf capacitor. The amplifier plate circuit is returned to a variable voltage, which governs the limiting action. This arrangement should be capable of good operation between 1 and 10 MHz and at rf levels between 1 and 10 Vrms. Near 1 volt the operation is marginal; at higher levels the limiting action is predominant. For the experiments on lead, platinum, and tin, the frequencies were between 6 and 13 MHz and the rf levels used were around 3 Vrms.

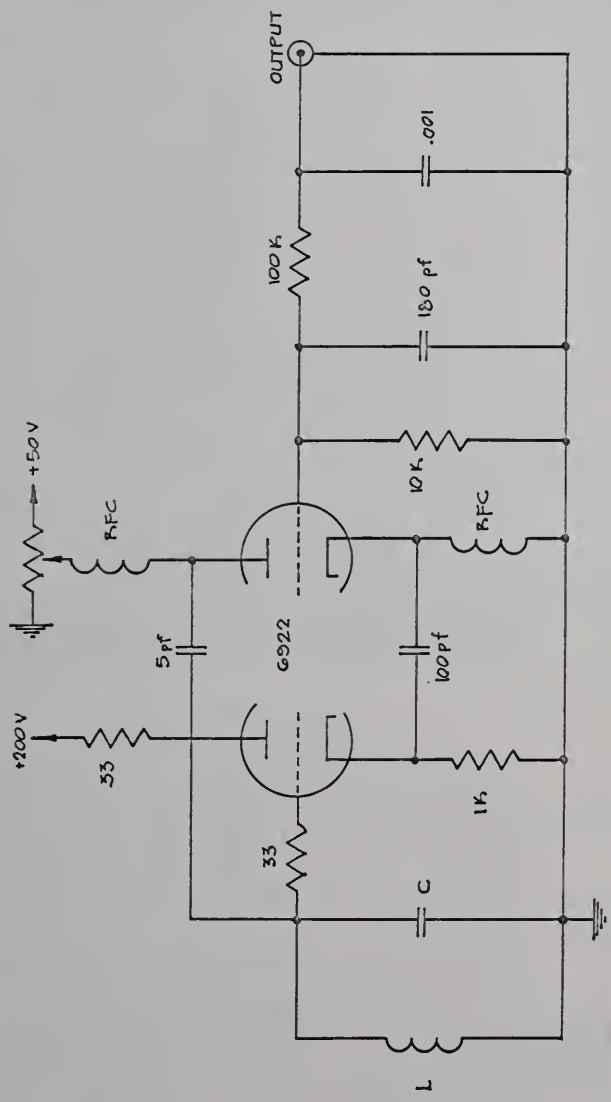

Figure 3. Basic circuit for high-level Knight oscillator.

The complete spectrometer, comprised of the Knight oscillator-detector, a calibrator (6C5), and a cathode follower (2C51) to match the impedance to that of the frequency counter, is shown in Figure 4. The primary purpose of the calibrator is to provide a non-saturable resonance in order to check the response of the remainder of the circuit. However in the experiments reported here, it was used in a different capacity. Due to the rather high modulation levels needed for the broad, weak metal resonances, there was considerable direct pickup of the modulation in the rf spectrometer, resulting in a large, constant ac signal at the spectrometer output. A signal the same frequency as the modulation but of variable phase was fed into the calibrator in order to cancel out the unwanted pickup.

Solid construction and good shielding of components is of major importance in constructing an NMR spectrometer. The chassis and shields for the spectrometer used here were formed out of 1/16-inch copper sheet. The shields were bolted in place in the chassis and then silver-soldered to the chassis and to one another to ensure rigidity. The shields were placed so that the various sections of the spectrometer (oscillator-detector, calibrator, counter circuit, filter network, and output network) were all individually enclosed by shielding. The components of the circuit were led through the shields by means of feed-through capacitors (about 2000 pf) in order to avoid leaving holes in the shields. Low-noise resistors were used where available. Of the various tubes tried in the oscillator-detector state, it was found that the 6922 gave the best signal-to-noise ratio. Both Amperex and RCA tubes were used, with the RCA giving perhaps slightly better results.

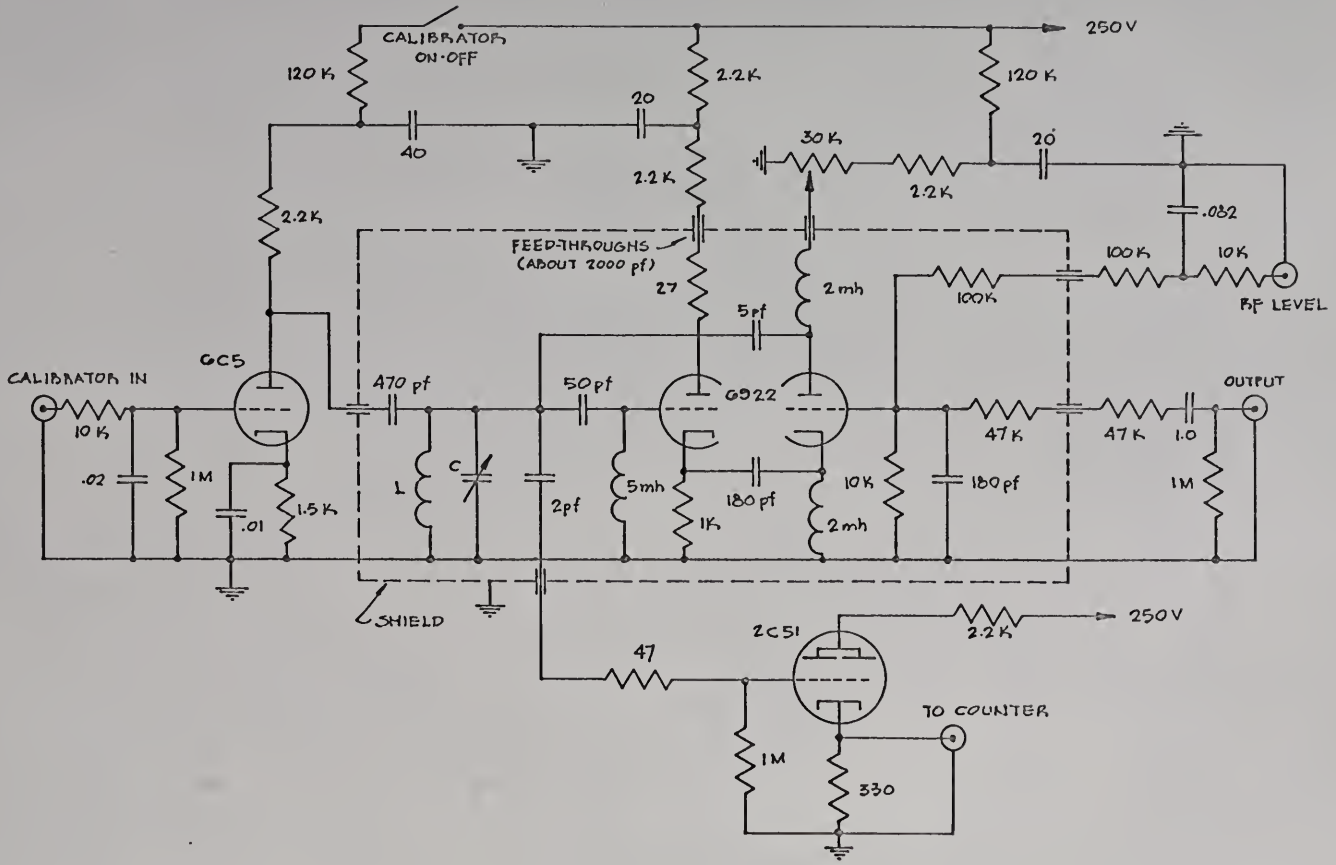

Figure 4. Spectrometer used for Knight shift studies.

Supporting electronics

A phase-shift unit and associated regulated power supply previously used by Brooker [37] were used to provide signals of variable phase and amplitude to the lock-in detector, to the calibrator tube in the spectrometer, and to the modulation amplifier. The circuit of the phase shifter is shown in Figure 5. An audio frequency was fed to the phase-shift unit by a Hewlett-Packard 201 C audio oscillator.

The modulation amplifier was a Williamson 20 watt high-fidelity power amplifier previously used by Haigh [38]. The circuit is shown in Figure 6. It was built to give a non-distorted, stable, hum-free modulation signal to the magnetic-modulation coils.

The filaments of the spectrometer were operated from a 6-volt lead storage battery in parallel with a battery charger. The B + power was supplied by a Lambda model 32 M regulated power supply. A Hewlett-Packard 524 D electronic counter was used to measure the rf frequency.

The lock-in amplifier (lock-in detector and narrow-band amplifier combined) was an Electronics, Missiles, and Communications, Inc. model RJB. No audio amplification was provided in the spectrometer, and the gain of the narrow-band amplifier was found to be not sufficient. So a Tektronix type 122 low-level preamplifier was inserted between the audio output of the spectrometer and the input to the narrow-band amplifier. The maximum gain available from the preamplifier was 1,000. The filaments of the preamplifier were operated from the same 6-volt storage battery as the spectrometer; however, the B + power was supplied by a pack of five 45-volt batteries (Eveready number 482).

The recorder used to display the resonances was a Honeywell Brown electronic recorder with a 10-0-10 mv sensitivity and a 2-second time

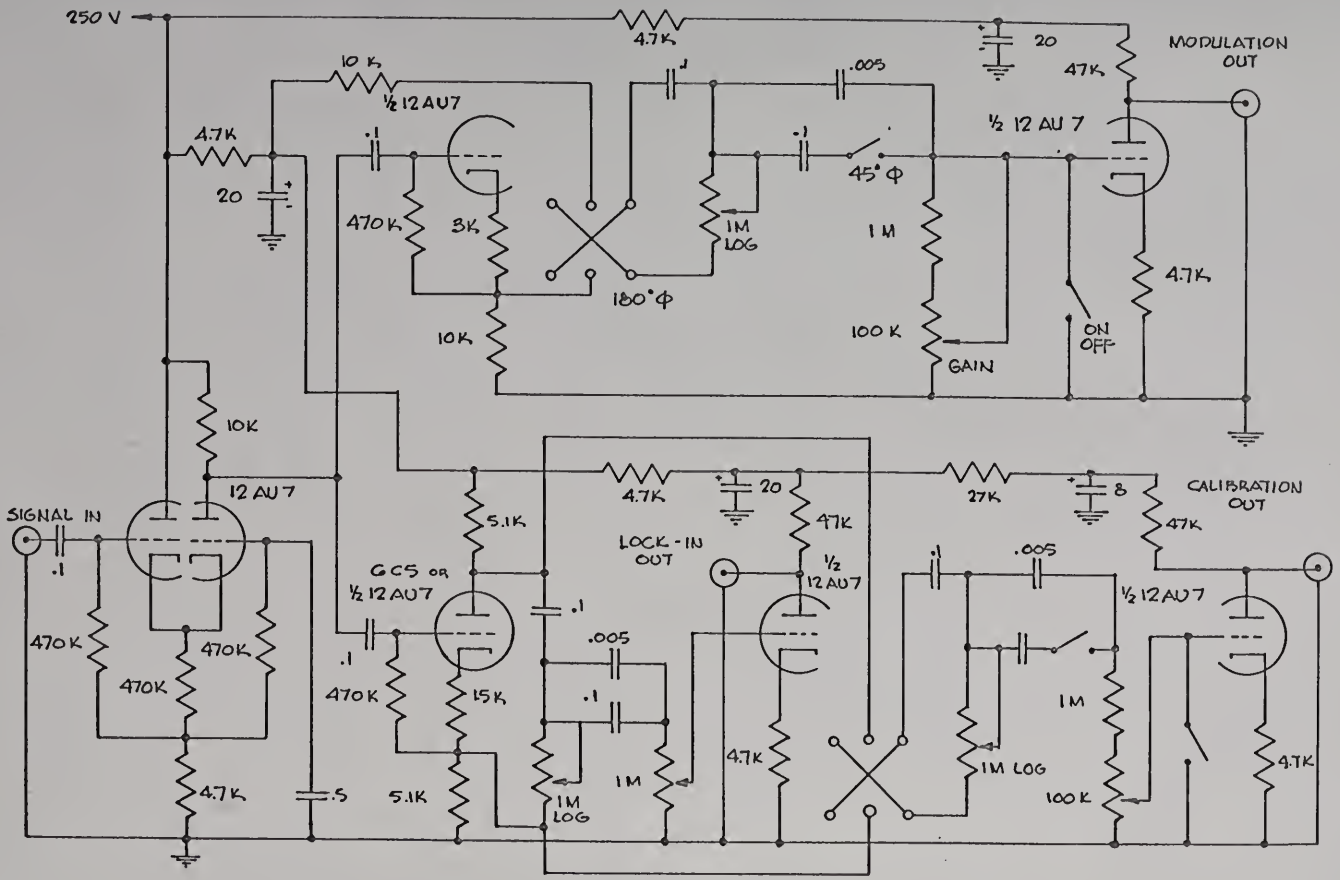

Figure 5. Phase-shift unit.

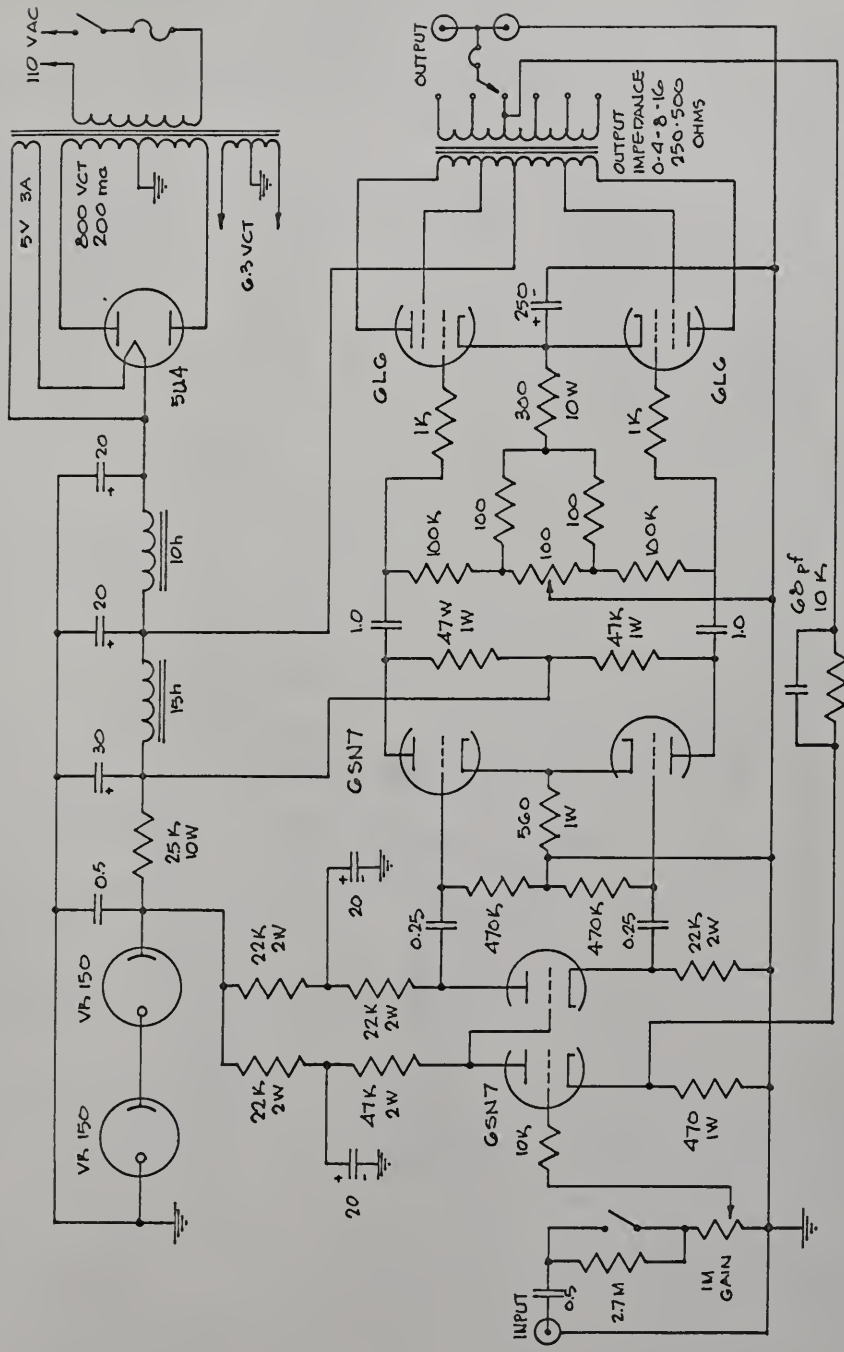

Figure 6. Modulation amplifier.

constant. The variable-speed clock drive used to drive the tuning capacitor of the spectrometer was a Harvard Apparatus Company model 600-000.

The magnet system

A Varian electromagnet with 12-inch diameter pole faces and a gap of 3 1/2 inches was used. The homogeneity of the field was measured using a five-section proton NMR probe [39]. It was found that the radial variation in the field could be described as $\Delta H = .16\ r^2$ where ΔH is the decrease in field (Oe) measured from the center of the gap at a field of H = 8,000 Oe and r is the radial distance from the center in inches.

Regulation of the magnet is important in these experiments, since the shifts in resonance frequency with pressure are quite small. To ensure good field stability, a Varian Fieldial Magnetic Field Regulator (model V-FR 2100), which employs the principle of the Hall effect, was utilized. A sensor probe containing a Hall crystal is attached to one of the pole faces within the magnet air gap. The sensor is excited by an oscillator in the Fieldial system, and when the magnetic field is present, an output voltage is obtained from the probe and applied to the sensing circuits. Any change in the field results in a corresponding change in the probe output voltage. This error voltage is applied to a phase-detector circuit in the Fieldial Regulator after amplification by an error amplifier. The phase-detected output is coupled to the magnet current-regulating system, causing the magnet current to change by the proper amount. A balanced condition is reached when the

magnetic field attains a value that produces no further change in the probe output voltage.

The manufacturer's specifications for the Fieldial Regulator are as follows:

(a) Field regulation

> Field intensity is held within 1 ppm, p-p, or 5 mOe, p-p, whichever is greater, for 10 per cent line voltage changes other than sharp changes.

(b) Field stability

> Field intensity is held within 1 ppm, p-p, of set field or 5 mOe, p-p, whichever is greater; band limited between .01 Hz and 1 Hz for conditions of 1 per cent line and 1° C water and ambient temperature change.

(c) Field ripple

> Less than 1 ppm, p-p, of set field, or 5 mOe, p-p, whichever is greater.

Several checks were made of the field-regulation system by measuring a deuterium NMR at regular intervals (about every half-hour) over a period of time. The frequency of resonance could be measured within an error of ± 10 Hz, which corresponds to a field of ± 15 mOe. It was found that the attachment of the sensor probe to the pole face is very important. When the adhesive supplied by the manufacturer to attach the probe was used alone, the probe had a tendency to pull away from the pole face resulting in a rather large drift in the field (about 3/4 Oe per hour). The situation was much improved by placing masking type on the probe to help hold it in place. During one run, the deuteron resonance remained within the measurable error of ± 10 Hz for 12 hours in a field of 7 kOe. During another run, a decrease in the field of 70 mOe (in a

field of 7 kOe) was observed over an eight-hour period. This drift could possibly be due to water or ambient temperature changes.

One important feature of the Fieldial regulating system compared to the ordinary current-regulating system is that in the former case, the field is not adversely affected by external magnetic disturbances, whereas it is in the latter case. This was dramatically demonstrated by moving a metal chair (used when taking data) a few feet in front of the magnet. Such movement caused the deuteron resonance to abruptly change by 50 Hz or so when the current-regulation system was used alone, but had no effect on the Fieldial system.

Two coils, each made of 46 turns of #28 enameled wire, were wound around the magnet pole pieces to provide the magnetic modulation. At a modulation frequency of 100 Hz the impedance of the coil is 16.5 ohms. The change in dc field produced by the coils per ampere at a field of H = 7,000 Oe is given by $\Delta H/\Delta I = 9.6$ Oe/amp.

High-Pressure Apparatus

The pressure system

A schematic diagram of the high-pressure generating system is shown in Figure 7. The 100,000 psi (pounds per square inch) and 200,000 psi pressure intensifiers were purchased from the Harwood Engineering Company, models B 2.5 and A 2.5 J respectively. These intensifiers are operated hydraulically by pumping oil at a relatively low pressure (0 to about 10,000 psi) into the lower end of the intensifier, forcing a piston upward. The pressure is multiplied through the piston by the ratio of the areas of the piston ends. The ratio of bottom area to

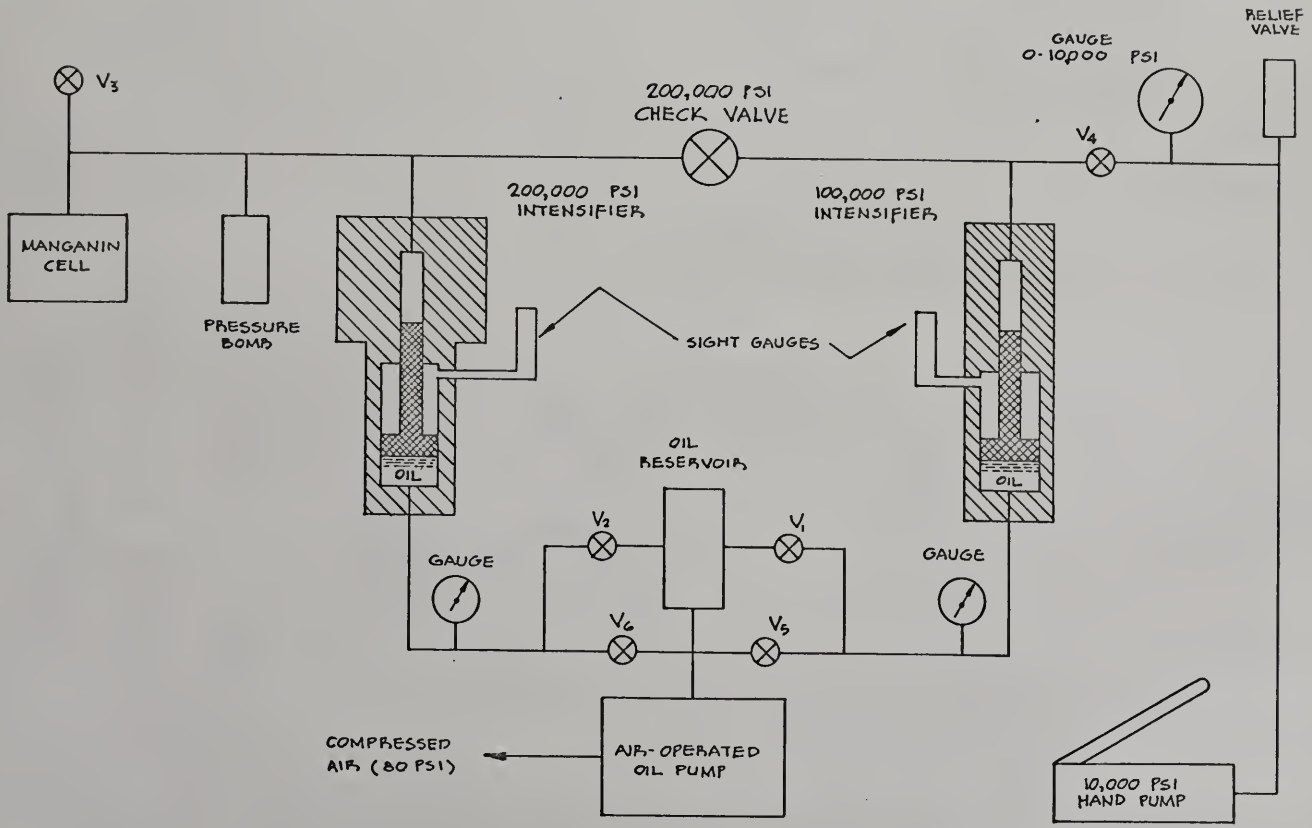

Figure 7. Schematic of 200,000 psi high-pressure system.

the top area is approximately 10.8-to-1 for the 100 kpsi intensifier and 15.5-to-1 for the 200 kpsi intensifier.

The hand pump is an Owatonna Tool Company model Y 21-1, and the 30,000 psi air-operated oil pump is from Sprague Engineering Corporation, model S-216 C. The 200 kpsi check valve and the various high-pressure fittings and tubing were also obtained from the Harwood Engineering Company.

The various components shown in the schematic were mounted on a portable stand having a base of 5/8-inch aluminum plate and a front and side shields of 1/4-inch aluminum plate. Back and front views of the complete system are pictured in Figures 8 and 9. The system was constructed so that the only components projecting through the front shield are the valves and gauges contained in the low oil-pressure part of the system. All of the high-pressure components are shielded from the front and sides by the aluminum plate. The overall system is 45 1/2 inches wide, 52 7/8 inches high (including 3-inch wheels), and 22 3/4 inches deep (from front to back).

The pressure-transmitting fluid used in these experiments was a three-to-one mixture of white gasoline-to-Octoil-S vacuum pump oil. White gasoline has been shown [40] to transmit pressure hydrostatically to pressures well over 200,000 psi at room temperature. The oil is added as a lubricant and rust inhibitor.

In actual operation, the pressure fluid is introduced into the reservoir of the hand pump, which is then used to charge the system with fluid. It is extremely important that all air be expended from the system during the charging process, since any gas trapped in the system would constitute a hazard at high pressures. After the initial

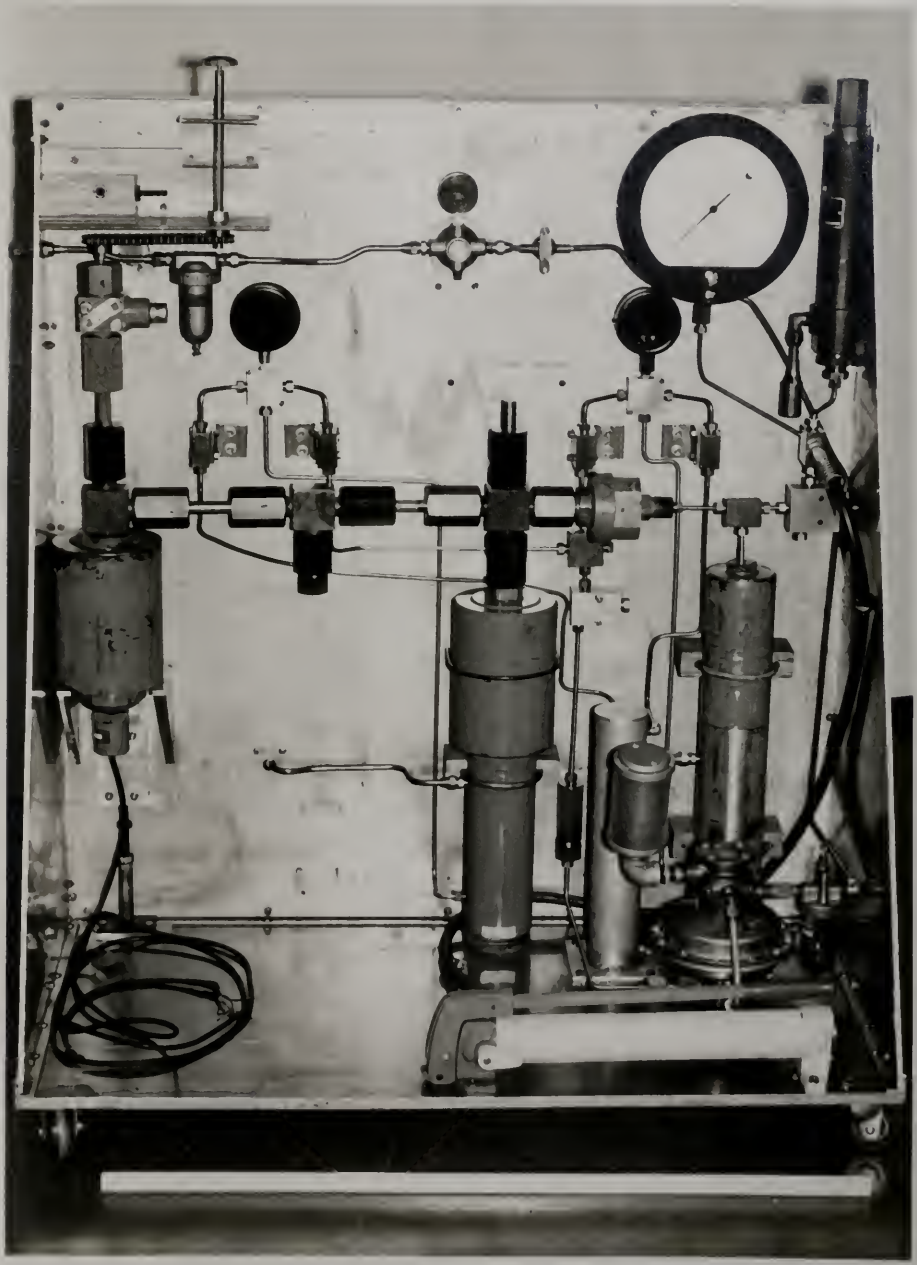

Figure 8. Back view of pressure system.

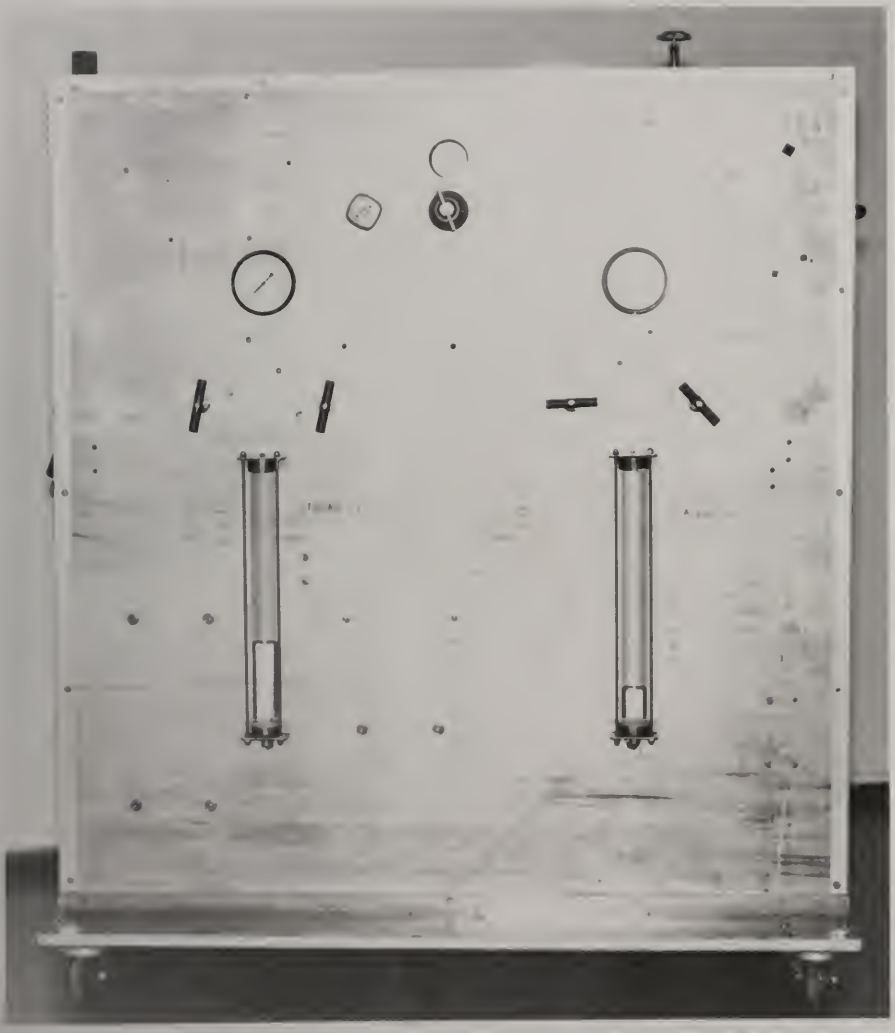

Figure 9. Front view of pressure system.

charging, bleed-off valves V_1, V_2, and V_3 are closed and the system is pumped up to about 8,000 psi with the hand pump. The hand pump and Heise gauge are then closed off from the rest of the system by closing valve V_4.

The 100 kpsi intensifier is activated by introducing compressed air into the air-operated oil pump and opening valve V_5 in the low-pressure oil system. The pressure is increased to 100 kpsi with this intensifier. It is then closed off by closing valve V_5, and valve V_6 is opened to activate the 200 kpsi intensifier. As the pressure is increased by this intensifier, the check valve automatically closes, isolating the 200 kpsi portion of the system. The pressure can now be increased to 200,000 psi.

At the completion of the experiment, the pressure is released by opening the bleed-off valves V_1 and V_2 in the low-pressure oil system, allowing the pistons to recycle downward and the oil to return from the intensifiers to the oil reservoir. Any remaining pressure can then be released by opening bleed-off valve V_3.

The pressure is measured by means of a Manganin Cell (from Harwood Engineering Company) containing a coil of manganin wire. The resistance of this wire is a linear function of pressure and is monitored by a Foxboro Dynalog Recorder model 9420 T, which records the pressure directly in pounds per square inch. The pressure can be read to an accuracy of about ± 0.5 per cent.

The pressure bomb

The pressure bomb and plug are shown in Figure 10. A non-magnetic pressure vessel is required, since the NMR experiment normally requires

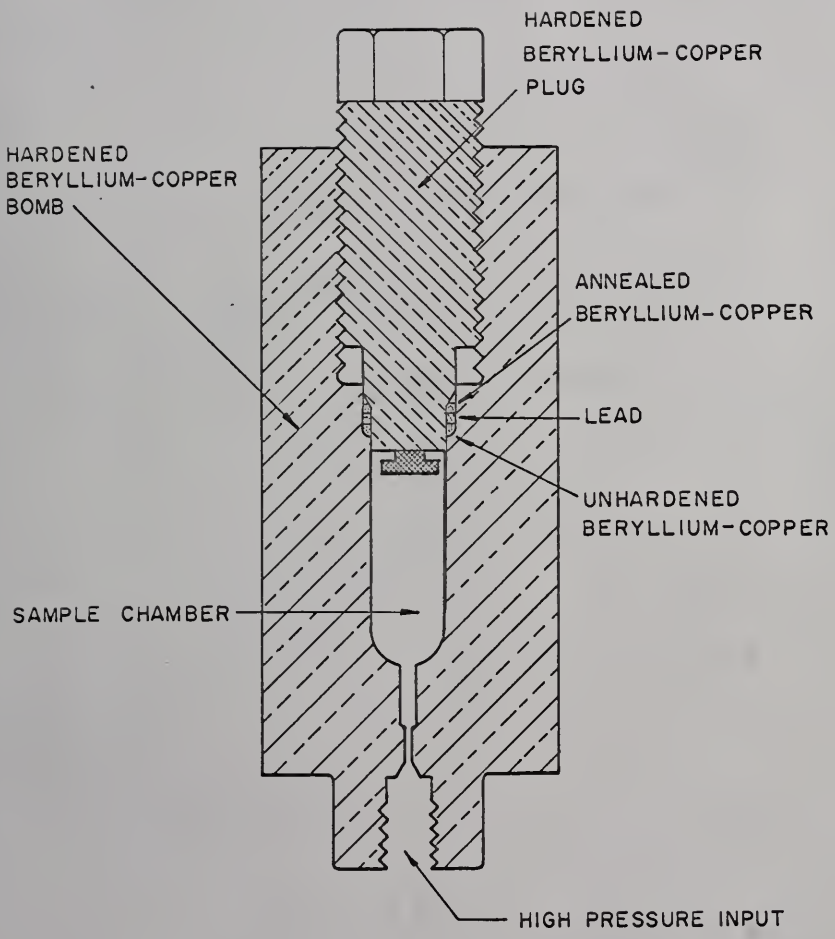

Figure 10. Pressure bomb and plug used at 200,000 psi. Full scale.

the application of a magnetic field. It has been found [41] that Berylco 25, a precepitation-hardening alloy of beryllium and copper, may be used successfully for this purpose. After machining, the material is hardened by heat treating at 600° F for three hours. The hardness of the vessel was tested and found to be Rockwell C-45. The bomb used in these experiments was composed of a 1.3-inch diameter inner cylinder interference fitted into a .35-inch thick sleeve by cooling the inner cylinder and heating the sleeve. This provided an initial stress in the bomb of about 30,000 psi. The sample chamber is 1/2 inch in diameter.

The plug is sealed into the bomb with plug seals utilizing the unsupported-area principle [42]. In this case three washers were used; the top one being annealed beryllium-copper is deformable against the hardened plug. The top face of this washer is an "unsupported area." The washer is crowded by the pressure into contact with the conical shoulder of the plug and out against the containing walls, in such a way that the intensity of pressure in the regions of contact is always greater than the intensity of pressure in the fluid contained in the bomb, thus preventing leakage. Evidently some flow in the washer is necessary before sealing takes place. The purpose of the middle washer, made of lead, is to provide the initial sealing until the top washer is sufficiently deformed to seal by the unsupported-area principle. The bottom washer, made of unhardened beryllium-copper simply serves as a spacer.

An electrical lead for one end of the rf coil is brought into the sample chamber through the plug by means of the electrical seal shown in Figure 11. Here it is necessary for the wire to be insulated from

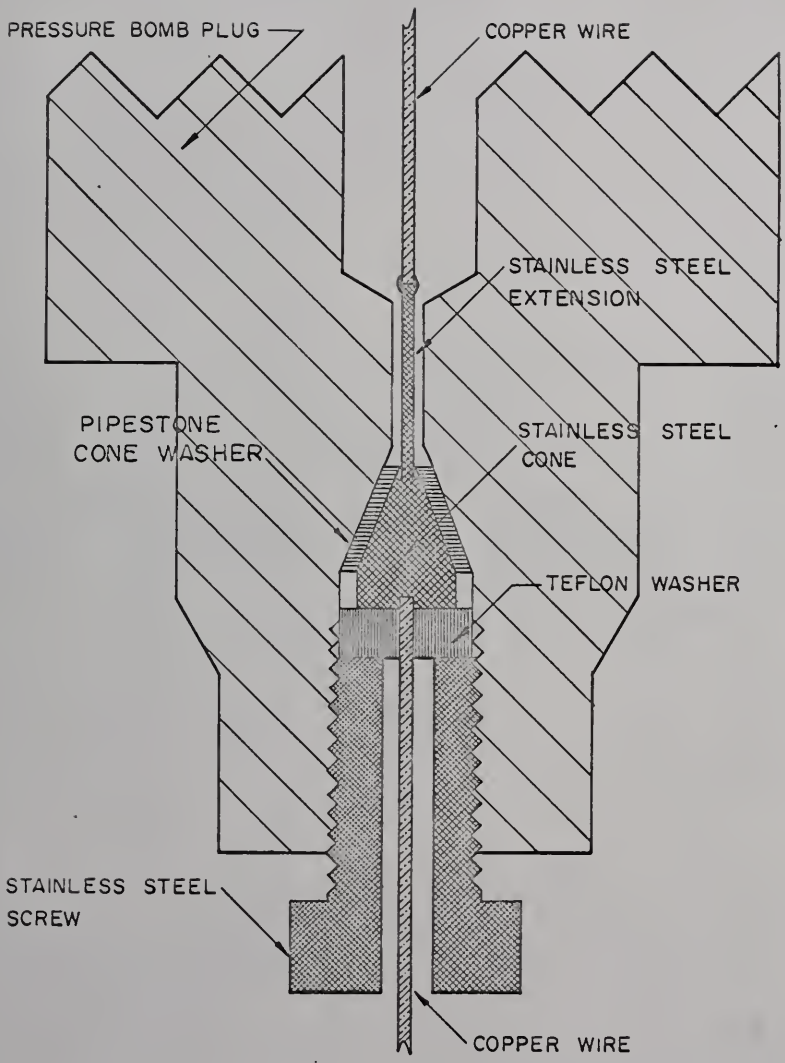

Figure 11. Electrical seal assembly used at 200,000 psi.
Scale: 5 times actual size.

the plug since the bomb and plug are connected into the ground of the electrical apparatus and the other end of the rf coil is soldered to the plug. The unsupported-area principle is again utilized with the cross section of the small plug hole being the unsupported area in this case. Insulating cone washers made of KEL-F were tried but found to be unsatisfactory at pressures above 100,000 psi due to excessive flow into the small plug hole. The bomb and seals used in these experiments were satisfactorily tested to pressures of 200,000 psi.

Experimental Technique

The metal samples

As has been mentioned previously, NMR experiments in metals are usually performed on powdered samples because of the skin-depth effect in metals. In order to ensure adequate penetration of the rf field into the sample and to avoid distorting the line shape and shifting the center due to eddy-current effects, the ratio D/δ should be less than one. Here D is the particle diameter and δ is the skin depth.

The metals used were purchased in the form of powders (sponge in the case of platinum) and sieved through a 325-mesh sieve to obtain the smallest particles. The mesh opening of the sieve is 43 microns; however, the average particle size was probably somewhat smaller than this value. The skin depths [43] at 20° C and the frequencies used in the experiment (7 MHz for lead and platinum, 10.5 MHz for tin), and the D/δ ratios for a 43 μ particle size are as follows:

$\delta(Pb) = 90\ \mu$	$D/\delta = .48$
$\delta(Pt) = 60\ \mu$	$D/\delta = .79$
$\delta(Sn) = 53\ \mu$	$D/\delta = .81$.

The magnitude of the shift in frequency due to eddy currents [44] is proportional to the linewidth and for $D/\delta = 1$ and a linewidth of 3.5 kHz amounts to only 30 Hz. This is somewhat less than the measured errors in the NMR frequencies, as will be seen in the next chapter.

The platinum sample (99.999 per cent pure) was purchased from the Leytess Metal and Chemical Company and the tin sample (99.9 per cent pure) from A. D. Mackay, Incorporated. The lead sample (99.99 per cent pure) was supplied by the Metallurgy Department at the Univeristy of Florida.

Experimental procedure

The metal samples were sieved into a pool of the pressure-transmitting fluid in order to obtain a good suspension of the metal particles in the fluid. In the case of lead and tin, the particles were covered with a layer of natural oxides, which provided sufficient electrical insulation of the individual particles from one another. However, the low reactivity of platinum prevented the formation of such a layer. It was found that as pressure was applied to the platinum sample, the rf level of the oscillator dropped to zero and the noise level of the oscillator increased. Such behavior was attributed to the platinum particles contacting one another electrically. This problem was overcome by mixing the platinum powder with alumina (Al_2O_3) powder. In order to reach the pressures used in the experiment (180,000 psi), it was found necessary to use an alumina-to-platinum ratio of two-to-one. The addition of the alumina powder did not affect the resonance

frequency or the line shape, as was demonstrated by comparing to pure platinum at atmospheric pressure.

The rf coil for the experiments was made by winding wire on a suitable form and then applying epoxy in several places to hold the winding together. After the epoxy had dried, the coil was slipped off the form and the sample placed inside. The coil was then covered with cloth on both ends and around the circumference to hold-in the sample powder. Such an arrangement allowed complete penetration of the pressure fluid into the sample. The coil was then mounted on the plug of the pressure bomb and sealed into the bomb.

In the performance of the experiment, the bomb was placed in the gap of the electromagnet and connected to the pressure-generating facility by means of Harwood 3-M pressure tubing. Such tubing is capable of withstanding pressures well in excess of 200,000 psi. The tubing was attached to the bomb with non-magnetic fittings (beryllium-copper and stainless-steel) and a thermometer was taped to the side of the bomb to measure the temperature. The magnet gap was enclosed on the top and front with 1/2-inch aluminum plate as a protective measure against bomb failures.

Because of large eddy-current effects in the beryllium-copper pressure bomb, low-frequency (30 Hz) modulation was used for all runs. Rather large modulation levels had to be used because of the broad resonances (3 to 5 kHz) and the weak signals obtained from the samples within the bomb, although the levels were kept as low as possible to minimize modulation broadening. However, the combination of large modulation amplitude and low frequency affected the operation of the Fieldial field-regulating system so that its sensitivity had to be reduced.

In order to continually monitor the field and account for any drift due to the reduced sensitivity of the Fieldial, a deuterium sample was placed in the field about 1/4 inch in front of the pressure bomb. The resonance of this sample was measured before and after every metal resonance. The time of each resonance (D_2O and metal) was noted and at the completion of a run, all resonances were plotted against time. By this method, corrections could be made for any field changes that occurred during the experiment. The deuterium resonance could be measured to about ± 10 Hz, thus allowing compensation for field changes corresponding to ± 15 Hz for lead and platinum and ± 25 Hz for tin.

Data reduction

The resonance frequency was measured as a function of pressure and was then used to compute the pressure dependence of the Knight shift from the formula

$$K(P) = \frac{\nu(P)-\nu(0)}{\nu(P)} [1+K(0)]+K(0) \qquad (103)$$

where $\nu(P)$ is the resonance frequency at pressure P, $\nu(0)$ is the frequency at atmospheric pressure, and $K(0)$ is the Knight shift at atmospheric pressure, assumed known. This is derived by assuming that the Knight shifts are given by

$$K(0) = \frac{\nu(0)-\nu_r}{\nu_r} \qquad (104a)$$

$$K(P) = \frac{\nu(P)-\nu_r}{\nu_r} \qquad (104b)$$

where ν_r is the resonance frequency in some reference compound. In

the case of lead and platinum, $\nu(0)$ and $\nu(P)$ are taken to be the zero crossing of the resonance derivative; while for the isotropic Knight shift in tin, they are taken to be $\nu_\perp + 1/3(\nu_{||} - \nu_\perp)$ where $\nu_{||}$ and $\nu_\perp$ correspond to the furthest points of maximum slope of the absorption curve (as discussed in the previous chapter).

The pressure dependence of the anisotropic Knight shift in tin is computed from the formula

$$K_{ax}(P) = \left[\frac{\delta(P)-\delta(0)}{\delta(0)} + 1\right] K_{ax}(0) \qquad (105)$$

where $\delta = 1/3(\nu_{||} - \nu_\perp)$ and $K_{ax}(0)$ is the known anisotropic Knight shift at atmospheric pressure. This is derived by assuming that the anisotropic Knight shifts are given by

$$K_{ax}(0) = \frac{\delta(0)}{\nu_r} \qquad (106a)$$

$$K_{ax}(P) = \frac{\delta(P)}{\nu_r} \; . \qquad (106b)$$

The volume dependences of the Knight shifts can be deduced from the pressure dependences by using the appropriate compressibility. These are given by Bridgman [42] as

$$\beta \text{ (lead)} = 2.42 \times 10^{-12} \text{ cm}^2/\text{dyne}$$

$$\beta \text{ (platinum)} = .367 \times 10^{-12} \text{ cm}^2/\text{dyne}$$

$$\beta \text{ (tin)} = 1.91 \times 10^{-12} \text{ cm}^2/\text{dyne} \; .$$

The volume compressibility for tin is taken to be $\beta = 2\beta_\perp + \beta_{||}$.

CHAPTER IV

RESULTS AND CONCLUSIONS

The Knight Shift in Lead

The resonant frequency of ^{207}Pb was measured up to pressures of 12,350 bars (179,000 psi) at 26° C. An example of the resonance derivative is shown in Figure 12. The linewidth was approximately 3,500 ± 400 Hz (uncorrected for modulation broadening), and remained constant within experimental error at all pressures. As well as could be determined, the resonance line also remained symmetric at all pressures. As can be seen from Figure 12, the signal-to-noise ratio was not very good. This fact, along with the rather broad line, precluded an accurate determination of the line center.

One of the interesting features of the lead experiment is the very small change in resonance frequency, even at the highest pressure. At 12,350 bars, the frequency increases only 240 ± 170 Hz out of about 7.2 MHz. This leads to a percentage change in the Knight shift of + .22 ± .2 per cent. The resonance was repeated several times at atmospheric pressure and at high pressures; the above numbers represent the averages of these measurements. Figure 13 shows the volume dependence of the Knight shift in ^{207}Pb at 26° C, deduced from the pressure measurements as discussed at the end of Chapter III. The Knight shift at atmospheric pressure was taken to be 1.47 per cent [45]. Measurements were not taken at lower pressures because the

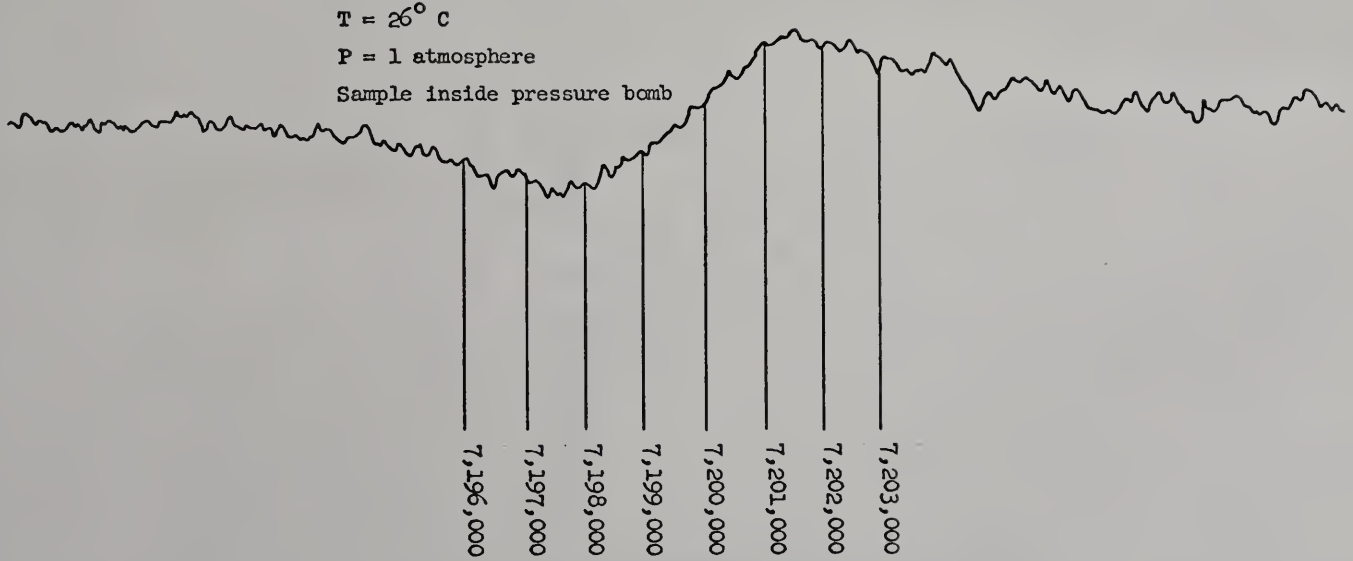

Figure 12. Nuclear magnetic resonance of ^{207}Pb in metallic lead.

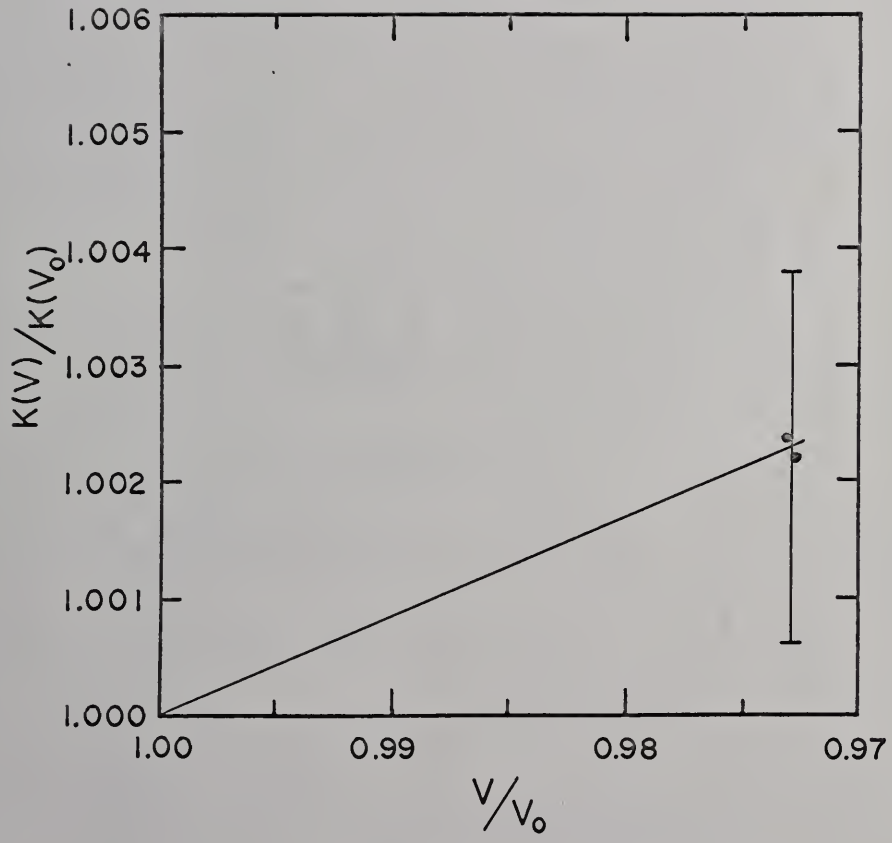

Figure 13. Volume dependence of the Knight shift in lead at 26° C.

pressure shift was too small to measure. For computational purposes, the volume dependence is expressed in terms of V^{α} with the result

$$\frac{K(V)}{K(V_o)} = \left(\frac{V}{V_o}\right)^{-.08 \pm .06} \tag{107}$$

where V_o is the volume at atmospheric pressure.

The temperature dependence at constant atmospheric pressure has been measured by Feldman [19]. His results give

$$\left(\frac{\partial \ell nK}{\partial T}\right)_P = .86 \times 10^{-4}\ K^{-1} . \tag{108}$$

As was mentioned in Chapter II, this temperature dependence is composed of a contribution due to the volume changes accompanying the temperature variation, and also an explicit dependence on temperature at constant volume. The former contribution can be computed from the measured volume dependence and the known thermal expansion (87×10^{-6} K^{-1} [46]). This gives for the contribution from thermal expansion

$$\left(\frac{\partial \ell nK}{\partial \ell nV}\right)_T \left(\frac{\partial \ell nV}{\partial T}\right)_P = -.07 \pm .05 \times 10^{-4}\ K^{-1} . \tag{109}$$

Thus, for lead, we have for the explicit temperature dependence at constant volume

$$\left(\frac{\partial \ell nK}{\partial T}\right)_V = .93 \pm .05 \times 10^{-4}\ K^{-1} . \tag{110}$$

We see then that the Knight shift in lead does indeed depend explicitly on the temperature, and it is comparable in magnitude to the explicit temperature dependence deduced by Benedek and Kushida for the alkali metals [16]. However, contrary to the situation in the alkalis, the explicit temperature dependence for lead is an order of magnitude larger than the contribution from thermal expansion.

In order to apply the hypothesis of Benedek and Kushida for an explicit temperature dependence caused by lattice vibrations, we must deduce the volume dependence of P_F from the pressure data. This is done by first calculating the volume dependence of $\chi_P\Omega$ according to the collective-electron picture of Pines. The crystal structure of lead is fcc, and the lattice constant is 4.9505 Å [47]. The number of conduction electrons per atom is taken as four. From these data, the inter-electronic spacing is calculated to be $r_s = 2.3$ Bohr units. For the small changes in r_s which are produced during compression to 12 kilobars, it is found possible to write the volume dependence of $\chi_P\Omega$ as a power dependence on the volume. The result for lead using equations (90) to (94), is

$$\frac{\chi_P(V)\Omega(V)}{\chi_P(V_o)\Omega(V_o)} = \left(\frac{V}{V_o}\right)^{.7} . \qquad (111)$$

In this calculation, m^*/m was taken to be one; however the volume dependence of $\chi_P\Omega$ is not sensitive to the particular value chosen for the effective mass.

As was shown previously, the free-electron model would predict a dependence of the 2/3 power of V/V_o. The result here thus compares quite closely with the free-electron model. This is consistent with de Haas-van Alphen studies, which have shown the Fermi surface in lead to conform very closely to a nearly free-electron Fermi surface based on four conduction electrons per atom [48].

Combining equations (107) and (111), we get for the volume dependence of P_F

$$\frac{P_F(V)}{P_F(V_o)} = \left(\frac{V}{V_o}\right)^{-.78\pm.06} . \qquad (112)$$

This volume dependence is also comparable in magnitude to that obtained by Benedek and Kushida for the alkalis [16]. From the discussion in Chapter II, we have for the explicit temperature dependence of the Knight shift

$$\left(\frac{\partial \ell nK}{\partial T}\right)_V = \tfrac{1}{2}\left(\frac{\partial^2 P_F(V)/P_F(V_o)}{\partial(V/V_o)^2}\right)_{V_o} \frac{\beta k}{\Omega} \ . \qquad (113)$$

For lead we have $\Omega = 30 \times 10^{-24}$ cm^3, and

$$\beta = 2.42 \times 10^{-12} \text{ cm}^2/\text{dyne} \qquad (114)$$

for the compressibility [42]. Thus,

$$\left(\frac{\partial \ell nK}{\partial T}\right)_V = .08 \times 10^{-4} \text{ K}^{-1} \ . \qquad (115)$$

We see that this is an order of magnitude less than the measured explicit temperature dependence given by equation (110). One might try to explain the discrepancy in terms of the approximate nature of the calculation of the volume dependence of $\chi_P\Omega$. However, a volume dependence some five times stronger than that given by equation (111) would be required. This does not seem acceptable, especially in light of the agreement of the calculation with the proposed free-electron behavior of the conduction electrons in lead.

A close examination of equation (113) gives a clue as to the reason for the disagreement between theory and experiment for lead, in contrast to the good agreement obtained for the alkali metals. The explicit temperature dependence given by equation (113) depends directly on the compressibility, β. For lead, the compressibility is an order of magnitude less than the compressibility in the alkali metals, thus resulting in a much smaller calculated explicit temperature dependence

for a comparable volume dependence of P_F. It appears, then, that the Benedek and Kushida theory is quantitatively too simple to account for the explicit temperature dependence in lead.

Muto, et al. [33] have done a detailed theoretical study of the effect of lattice vibrations on the Knight shift, and find that an explicit dependence on temperature comes out of a general reformulation of the Knight shift in a vibrating lattice. They take into account not only the effect of the vibrations on the charge distribution of the conduction electrons (essentially Benedek and Kushida's approach), but also the effect on the hyperfine interaction of a conduction electron with a vibrating nuclear spin, and then a coupling of these two mechanisms, which gives a large contribution to the final numerical results. In applying their theory to the alkali metals, they find the resulting explicit temperature dependences are comparable in magnitude to Benedek and Kushida's for the lighter metals, but are an order of magnitude larger for the heaviest alkali (^{133}Cs).

It thus appears that the mechanisms examined by Muto, et al. could be large enough to explain the order of magnitude discrepancy between the calculated explicit temperature dependence in lead based on Benedek and Kushida's simplified approach, and the measured value. This might be especially true for lead, since the electron-phonon interaction is known to be strong [48].

It might be worthwhile to point out that Knight shift mechanisms other than the ordinary s-electron hyperfine interaction are probably unimportant in lead. As was mentioned previously, the Fermi surface in lead has been examined in some detail using the de Haas-van Alphen

effect, and is found to conform quite closely to a nearly free-electron model with four conduction electrons per atom. We would thus expect the Pauli susceptibility to be a good approximation for the conduction electrons

$$\chi_P = \beta^2 N(E_F) \quad . \tag{116}$$

The density of states $N(E_F)$ was deduced by Anderson and Gold in the de Haas-van Alphen studies mentioned above to be

$$N(E_F) = 7.6 \text{ ry}^{-1} \text{ atom}^{-1} \quad . \tag{117}$$

As Anderson and Gold point out in their paper, this value for the density of states is some 2.2 times smaller than that calculated from the electronic specific heat coefficient. It was also found that the differential properties of the Fermi surface obtained from the de Haas-van Alphen data were smaller than those obtained from cyclotron resonance experiments by the same factor of 2.2. This quantitative enhancement of the specific heat and cyclotron resonance results is suggested by Anderson and Gold to be a result of the electron-phonon interaction. Recent theoretical predictions [49] suggest that this interaction should manifest itself in the same way in the two phenomena, but should not affect the spin susceptibility. For this reason, the density of states given by equation (117) is used in calculating the Pauli susceptibility rather than that calculated from the specific heat coefficient. The result is

$$\chi_P = .087 \times 10^{-6} \frac{\text{emu}}{\text{gr}} \quad . \tag{118}$$

Using the hyperfine coupling constant given in Knight's article [11],

and equation (49) of Chapter II, the Knight shift is

$$K = 2.34\% \ . \tag{119}$$

It is interesting to note how this number compares to that for which $N(E_F)$ is calculated on a strictly free-electron basis [equation (85b), Chapter II]. The result for this case is

$$K = 2.7\% \ . \tag{120}$$

These calculations have been based on the ratio of the probability density in the metal to that in the free atom, ξ, being taken as one; whereas, if one assumes a ratio of about .7 (which is common in the literature), the above calculated Knight shifts agree quite closely with the accepted measured value of 1.47 per cent [45]. Deducing the density of states from the specific heat measurements gives a Knight shift of 5.9 per cent.

In regard to the Knight shift studies on lead alloys by Snodgrass and Bennett [20], it appears that volume effects are an order of magnitude too small to explain the shifts in the alloys. The volume change in going from pure lead to 80% Pb - 20% In is $\frac{\Delta V}{V} = -2.2\%$. The change in the Knight shift due to such a volume change computed from equation (107) is $\Delta K/K = .1\%$; whereas the overall change in the Knight shift reported by Snodgrass and Bennett for this concentration range is $\Delta K/K = 1.1\%$. We can thus conclude that volume effects are not an important factor in determining the Knight shift in these alloys.

The Knight Shift in Platinum

The NMR of ^{195}Pt was measured as a function of pressure up to 12,350 bars (179,000 psi) at 26° C. Figure 14 illustrates the

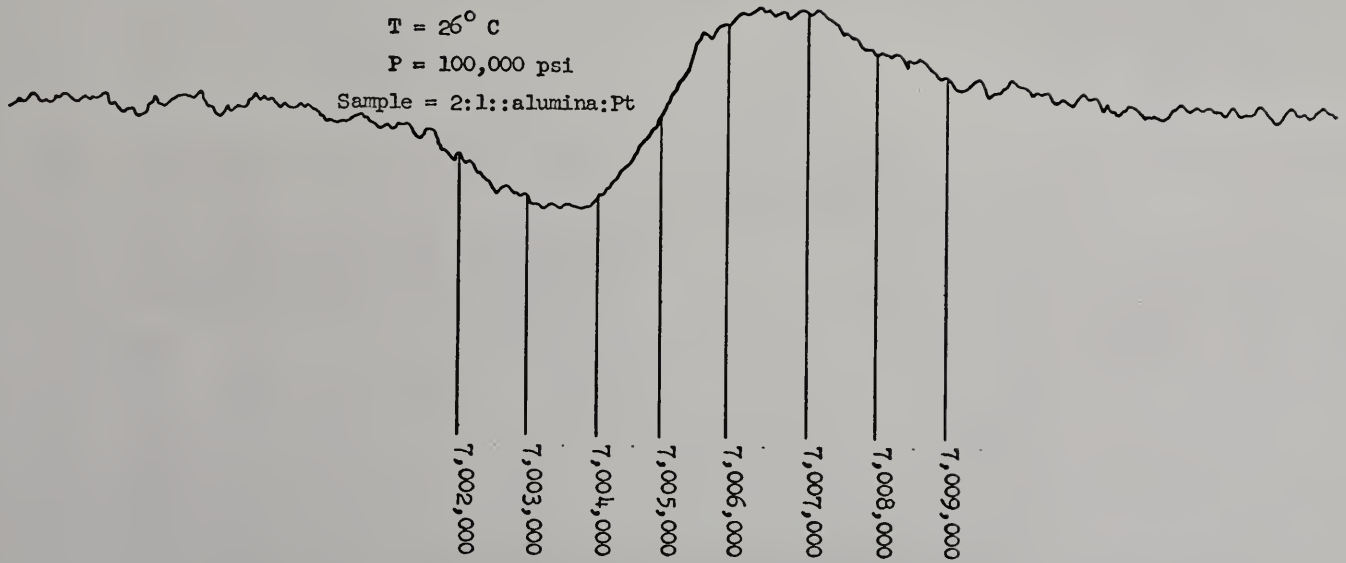

Figure 14. Nuclear magnetic resonance of ^{195}Pt in metallic platinum.

derivative of the resonance as displayed on the recorder. The line was symmetric and, as in the case of lead, both the shape and width of the line remained constant to the highest pressures. The peak-to-peak width of the observed derivative was about 3,100±200 Hz (uncorrected for modulation broadening). The linewidth reported by Rowland is 2.4 kHz [21]. The excessive width reported here is attributed to the high modulation level required in order to obtain a satisfactory signal-to-noise ratio.

Figure 15 shows the change in resonance frequency as the pressure is increased to a little over 12 kilobars. The frequency at atmospheric pressure was 7,004,800 Hz. The error flags represent the actual measured error in the zero point of the derivative tracing of about ± 50 Hz. The solid line indicated on the graph is the best fit to the experimental data. Several runs were made, with the data points all falling on the curve to within experimental error. The volume dependence of the Knight shift, taking the value at atmospheric pressure to be -3.52 per cent [21], is shown in Figure 16. It is seen that the dependence is quite close to being linear. A log-log plot results in the following volume dependence

$$\frac{K(V)}{K(V_o)} = \left(\frac{V}{V_o}\right)^{.99\pm.09} . \qquad (121)$$

The magnitude and direction of the volume dependence reported here at 26° C is in close agreement with that recently reported by Kushida and Rimai who measured the pressure dependence of the Knight shift in platinum at 64.8°, 0°, and -78.0° C [17].

On comparing the measurements here to the temperature dependence at constant pressure measured by Rowland [21], we find that the thermal-

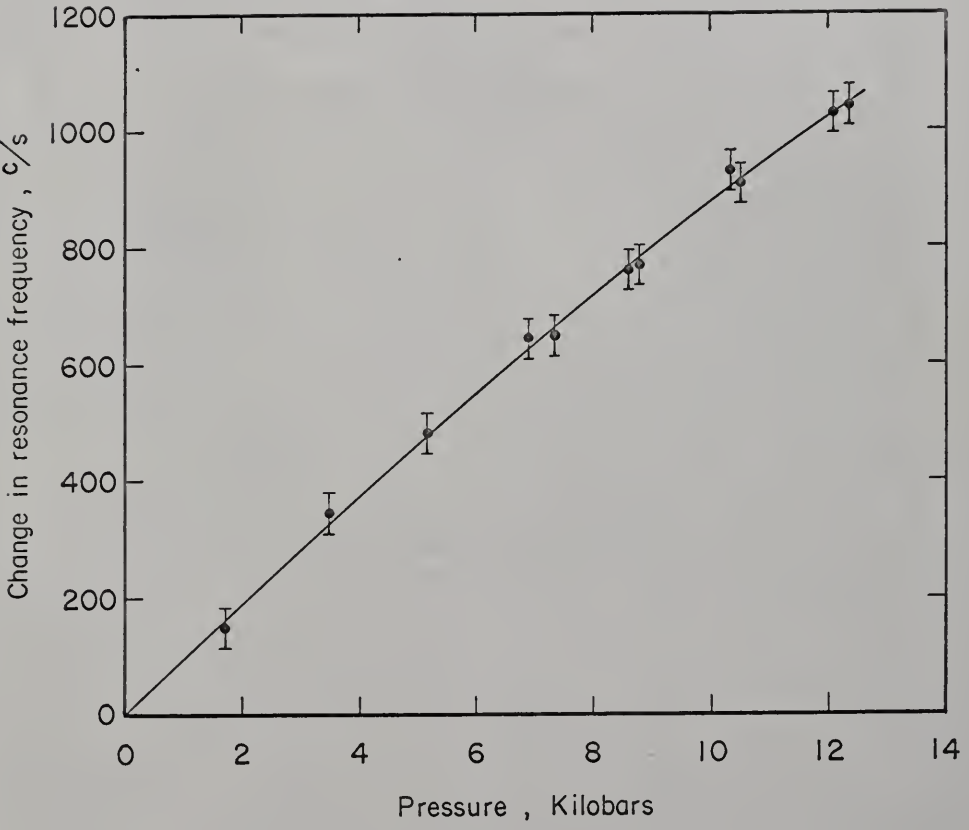

Figure 15. Pressure dependence of the resonance frequency in platinum at 26° C.

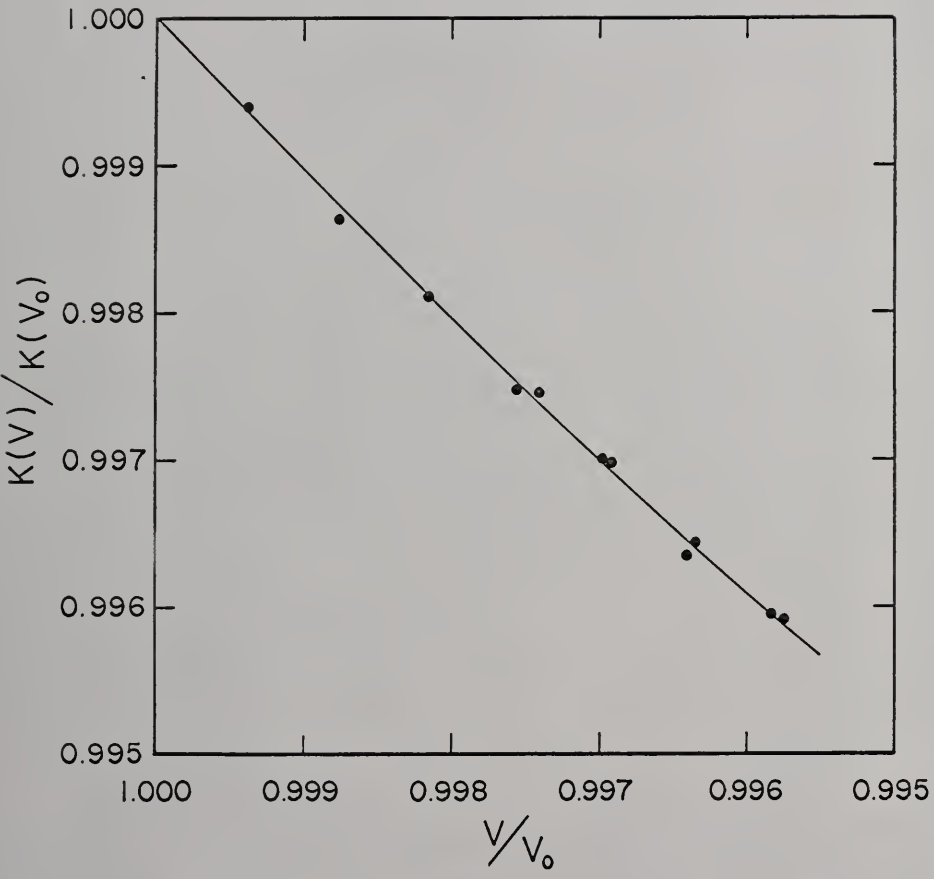

Figure 16. Volume dependence of the Knight shift in platinum at 26° C.

expansion contribution is quite small in comparison to the explicit temperature dependence at constant volume. The percentage change in the Knight shift as measured by Rowland is 15.3 per cent from 78° K to 350° K; whereas the percentage change due to thermal expansion over the same temperature range is only .72 per cent (the thermal expansion used here is $26.7 \times 10^{-6}\ K^{-1}$ [46]).

Of course, a large explicit temperature dependence for platinum is not unexpected, since the large negative Knight shift has been shown by Clogston et al. [22] to arise through core polarization from a large d-spin susceptibility. The susceptibility of the d-holes can be written

$$\frac{1}{\chi(T)} = \frac{1}{\chi_o(T)} - \frac{k_B T_{ex}}{n\beta^2} \tag{122}$$

where

$$\chi_o(T) = \frac{3n\beta^2}{2k_B T_d}\left[1 - \frac{\pi^2}{12}\left(\frac{T}{T_d}\right)^2\right]. \tag{123}$$

k_B is the Boltzmann constant, T_{ex} an effective exchange temperature, n is the number of d-holes per unit volume, and β is the Bohr magneton. The low degeneracy temperature of the d-holes (about 1,000° K) allows the susceptibility, and thus the Knight shift, to be strongly temperature dependent. The recent pressure work of Kushida and Rimai indicate that the explicit temperature dependence can be written in the form

$$K = K_o + K_1(T/T_d)^2 \tag{124}$$

consistent with the above formalism for the susceptibility.

The Knight Shift in Tin

The pressure dependence of the nuclear magnetic resonance in tin was measured up to 12,172 bars (176,500 psi) at 25° C. Both isotopes, ^{117}Sn and ^{119}Sn, were examined. The results for both isotopes were the same within experimental error, so only the data for ^{119}Sn will be given here. An asymmetric resonance was observed as expected, indicating the presence of an anisotropic Knight shift due to the non-cubic (tetragonal) crystal structure of tin. Figure 17 shows the observed resonance derivative for ^{119}Sn. The line shape is in good agreement with that reported by Bloembergen and Rowland [23], and Borsa and Barnes [24].

As was pointed out in Chapter II, the isotropic Knight shift is measured from a point two-thirds of the way from $\nu_{\parallel}$ to $\nu_{\perp}$, and the anisotropic shift is determined from the difference between $\nu_{\parallel}$ and $\nu_{\perp}$. Figure 18 shows the pressure dependence of the resonant frequency $\nu_o = \nu_{\perp} + \frac{1}{3}(\nu_{\parallel} - \nu_{\perp})$ in ^{119}Sn. The resonance frequency at atmospheric pressure was ν_o = 10,501,800 Hz. For the sake of clarity, the error flags have been omitted from the drawing; they amount to about ±175 Hz at each datum point. The straight line indicates the best fit to the data.

In Figures 19 and 20 are plotted the isotropic Knight shift, K_{iso}, and anisotropic Knight shift, K_{ax}, respectively, versus volume. The shifts at atmospheric pressure were taken to be K_{iso} = .75 per cent and K_{ax} = .025 per cent [24]. In both cases, the solid lines are the best fits to the experimental data. The volume dependences obtained from these data are

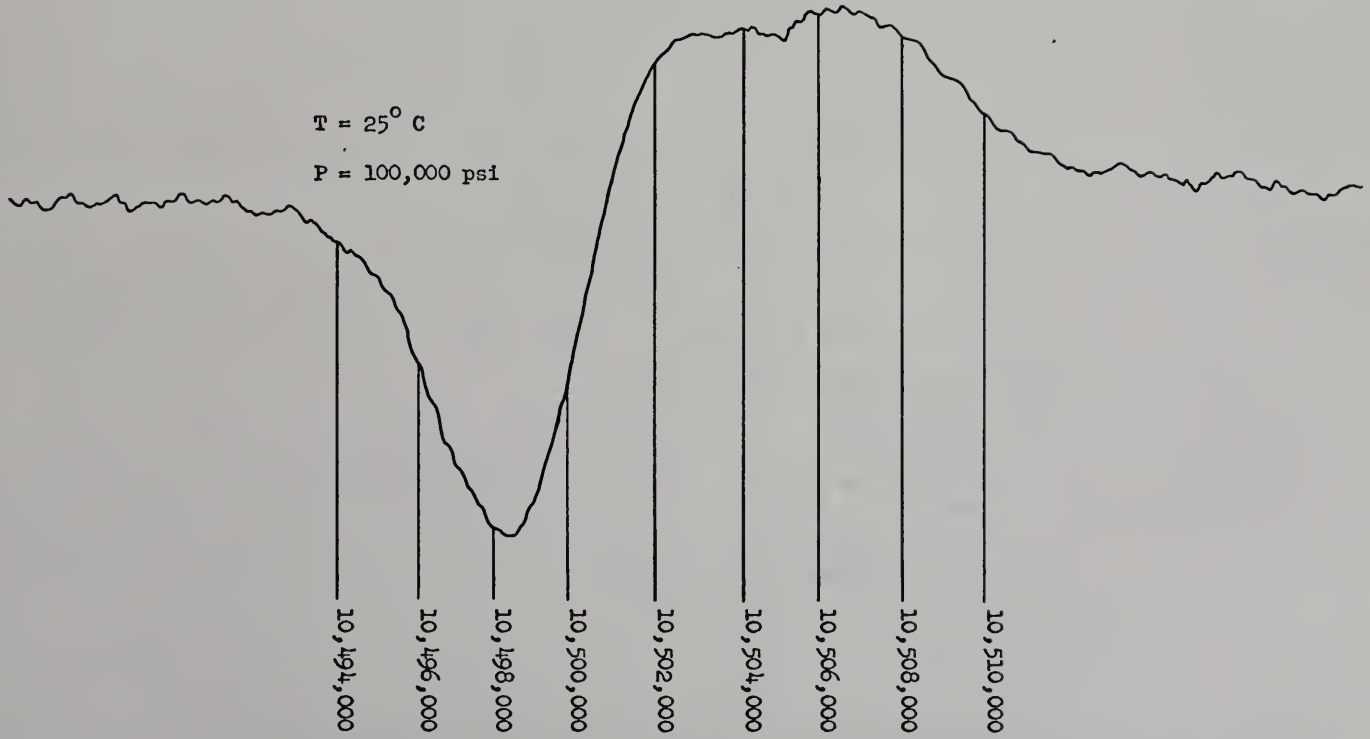

Figure 17. Nuclear magnetic resonance of ^{119}Sn in metallic tin.

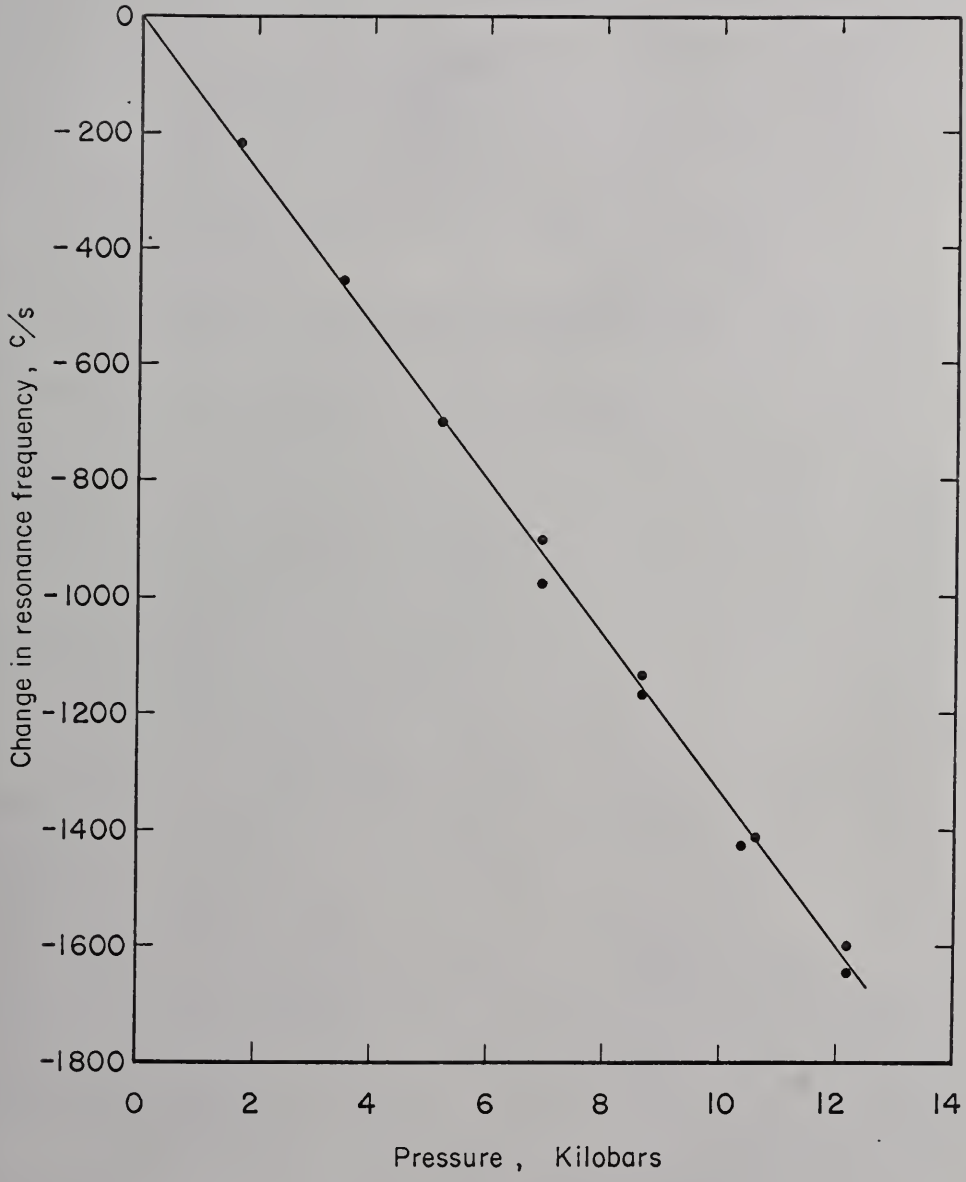

Figure 18. Pressure dependence of the center-of-gravity resonance frequency in ^{119}Sn at 25° C.

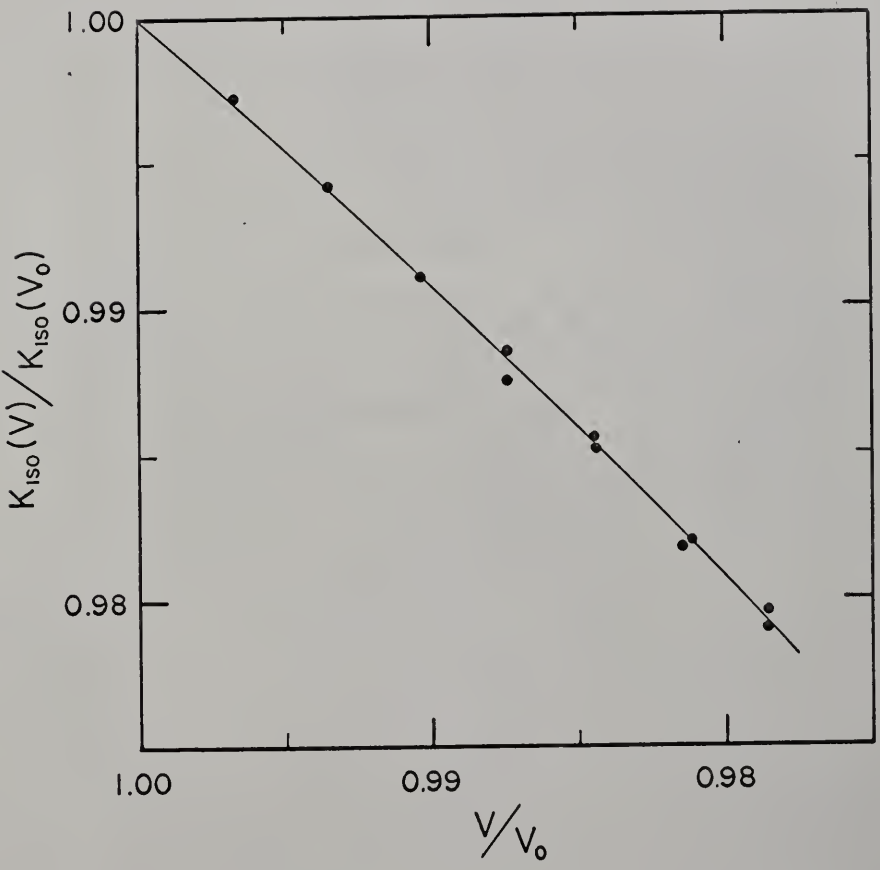

Figure 19. Volume dependence of the isotropic Knight shift in ^{119}Sn at 25° C.

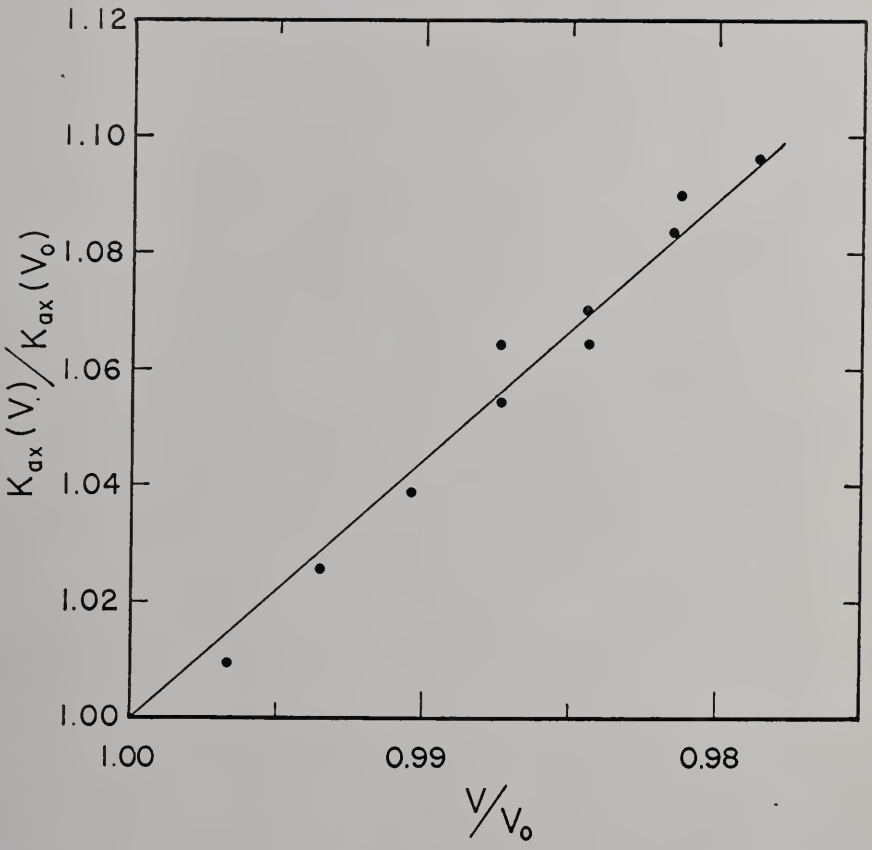

Figure 20. Volume dependence of the anisotropic Knight shift in ^{119}Sn at 25° C.

$$\frac{K_{iso}(V)}{K_{iso}(V_o)} = \left(\frac{V}{V_o}\right)^{.96\pm.06} \qquad (125a)$$

$$\frac{K_{ax}(V)}{K_{ax}(V_o)} = \left(\frac{V}{V_o}\right)^{-4.25\pm1.8} . \qquad (125b)$$

The rather large error in the volume dependence of the anisotropic Knight shift is due to the fact that the double peak in the high frequency side of the resonance is not very well defined, as can be seen in Figure 17, thus making the difference $\nu_{\parallel} - \nu_{\perp}$ somewhat difficult to determine. The above stated errors are actual measured errors; however, as can be seen from the good consistency in the data in Figure 20, the error in the case of K_{ax} is probably somewhat too liberal.

In their paper [24], Borsa and Barnes report values of the Knight shift at 300° K and 77° K, and give the percentage change in the Knight shift as

$$\frac{K_{iso}(300) - K_{iso}(77)}{K_{iso}(300)} = 2.3\% \qquad (126a)$$

$$\frac{K_{ax}(300) - K_{ax}(77)}{K_{ax}(300)} = -5\% . \qquad (126b)$$

Using the measured volume dependence, we can estimate the contribution from thermal expansion to these changes. Taking the thermal expansion for tin as $61.8 \times 10^{-6}\ K^{-1}$ [45], the volume change between 300°K and 77°K is

$$\frac{V(300) - V(77)}{V(300)} = 1.212\% . \qquad (127)$$

The corresponding changes in the Knight shifts are

$$\frac{K_{iso}(V_o) - K(V)}{K_{iso}(V_o)} = 1.2\% \qquad (128a)$$

$$\frac{K_{ax}(V_o) - K_{ax}(V)}{K_{ax}(V_o)} = -5\% \ . \qquad (128b)$$

It thus appears that the change with temperature of the anisotropic Knight shift can be fully accounted for by thermal expansion; whereas thermal expansion only accounts for about one-half of the change with temperature of the isotropic Knight shift. It should perhaps not be taken too seriously, since the errors involved in the measurements are quite large. For the rather small changes in K_{ax} associated with the above temperature and volume changes, the relative error in the measured change of K_{ax} is about ±100 per cent.

We might now try to compare the explicit temperature dependence in the case of K_{iso} to that calculated according to the hypothesis of Benedek and Kushida, as in the discussion on lead. The volume dependence of P_F is first deduced by calculating the volume dependence of $\chi_p\Omega$ according to the collective-electron picture of Pines. The crystal structure of tin is tetragonal with four atoms per unit cell having lattice constants a = 5.8197 and c = 3.1749 [47]. Assuming four conduction electrons per atom, the inter-electronic spacing is calculated to be r_s = 2.22 Bohr units. Using equations (90) to (94) and $m^* = m$, the volume dependence of $\chi_p\Omega$ is computed to be

$$\frac{\chi_p(V)\Omega(V)}{\chi_p(V_o)\Omega(V_o)} = \left(\frac{V}{V_o}\right)^{.65} \ . \qquad (129)$$

Using this and equation (125a) the volume dependence of P_F is found to be

$$\frac{P_F(V)}{P_F(V_o)} = \left(\frac{V}{V_o}\right)^{.31\pm.01} \ . \qquad (130)$$

Equation (113) is now used to calculate the explicit temperature

dependence. Using

$$\beta = 1.91 \times 10^{-12} \text{ cm}^2/\text{dyne} \tag{131}$$

and $\Omega = 27 \times 10^{-24}$ cm^3, the result is

$$\left(\frac{\partial \ln K_{iso}}{\partial T}\right)_V = -.01 \times 10^{-4} \text{ K}^{-1} . \tag{132}$$

A "measured" value of the explicit temperature dependence is obtained from the temperature data at constant pressure of Borsa and Barnes and the measured volume dependence, equation (125a). Using 61.8×10^{-6} K^{-1} as the thermal expansion of tin, we get

$$\left(\frac{\partial \ln K_{iso}}{\partial T}\right)_V = .43 \times 10^{-4} \text{ K}^{-1} . \tag{133}$$

We see that the theoretical value, equation (132), is much too small and of the wrong sign. In analyzing the possible causes of the disagreement, we note the form of the volume dependence of P_F as given by equation (130). Since the electron wave functions in P_F are normalized over the atomic volume, the volume dependence of P_F for free electrons is expected to be close to V^{-1}. This is the case for lead (discussed earlier in this chapter) and for most of the alkalis [16].

In attempting to put forth an explanation for the behavior of P_F in tin, we assume the electron wave function to be a simple admixture of s- and p-type wave functions of the form [50]

$$\psi(\vec{r}) \rightarrow a_s\phi_s + a_1\phi_{px} + a_2\phi_{py} + a_3\phi_{pz} \tag{134}$$

where

$$|a_s|^2 + |a_1|^2 + |a_2|^2 + |a_3|^2 = 1 . \tag{135}$$

For axial symmetry, we expect

$$\langle |a_1|^2 \rangle = \langle |a_2|^2 \rangle \equiv \eta \tag{136}$$

and we also define

$$\langle |a_s|^2 \rangle \equiv \epsilon \tag{137a}$$

$$\langle |a_3|^2 \rangle \equiv \zeta \ . \tag{137b}$$

Then the probability density at the origin is

$$\langle |\psi(0)|^2 \rangle = \epsilon \langle |\phi_s(0)|^2 \rangle \ . \tag{138}$$

We see that ϵ is a measure of the amount of s-character in the total wave function.

The isotropic Knight shift can now be written

$$K_{iso} = \frac{8\pi}{3} \chi_P \Omega \epsilon \langle |\phi_s(0)|^2 \rangle \ . \tag{139}$$

If we assume that $\langle |\phi_s(0)|^2 \rangle \sim V^{-1}$ from normalization, then the volume dependence of the Knight shift can be explained in terms of a changing in the s-character of the wave function with

$$\epsilon \sim V^{1.31} \ . \tag{140}$$

Assuming the lattice vibrations do not affect the character of the wave functions, and using $\langle |\phi_s(0)|^2 \rangle \sim V^{-1}$ instead of P_F in equation (113), we obtain for the calculated explicit temperature dependence

$$\left(\frac{\partial \ln K_{iso}}{\partial T} \right)_V = .1 \times 10^{-4} \, K^{-1} \ . \tag{141}$$

On comparing this result to the measured explicit temperature dependence, equation (133), we see that the sign of the dependence

is now in the right direction, although the computed value is still a bit low. This could perhaps be explained, as in the case of lead, in terms of the failure of the Benedek and Kushida hypothesis to account for all the effects of the lattice vibrations.

The proposal of a changing of the character of the wave function with pressure could also account for the opposite volume dependences of K_{iso} and K_{ax}. If the s-character decreases with decreasing volume, then the p-character would be expected to increase with decreasing volume. Since the anisotropic Knight shift depends on the p-character of the wave function, we might expect K_{ax} to also increase with decreasing volume, and this is what is indicated by experiment [see equation (125b)].

It should be noted, however, that K_{ax} does not give a direct measure of the non-s character itself, but rather is proportional to the anisotropy in the p-character of the wave function. In terms of the previously described expansion of the wave function, the anisotropic Knight shift can be written [50]

$$K_{ax} = \frac{2}{5} \chi_P \Omega \langle r^{-3} \rangle_p (\zeta - \eta) \qquad (142)$$

where $\langle r^{-3} \rangle_p$ is the average over the unit cell of r^{-3} for an electron in a p-state and at the Fermi surface; ζ and η are the coefficients of admixture squared for p_z and $p_x = p_y$ states respectively. Assuming $\langle r^{-3} \rangle_p \sim V^{-1}$ from normalization of the wave function and using equations (125b) and (129) for the volume dependences of K_{ax} and $\chi_P \Omega$, we get for the volume dependence of the anisotropy of the p-character

$$(\zeta - \eta) \sim V^{-4.6} \quad . \qquad (143)$$

This would correspond to the charge distribution of the p-electrons on the Fermi surface being elongated in the c-direction as the pressure is increased.

LIST OF REFERENCES

1. E. Purcell, H. Torrey, and R. Pound, Phys. Rev. 69, 37 (1946).

2. F. Bloch, W. Hansen, and M. Packard, Phys. Rev. 69, 127 (1946).

3. A. Abragam, The Principles of Nuclear Magnetism (Clarendon Press, Oxford, 1961).

4. C. Slichter, Principles of Magnetic Resonance (Harper and Row, New York, 1963).

5. G. Pake, "Nuclear Magnetic Resonance," in Solid State Physics Vol. 2, edited by F. Seitz and D. Turnbull (Academic Press Inc., New York, 1956).

6. E. Andrew, Nuclear Magnetic Resonance (Cambridge University Press, New York, 1955).

7. W. Knight, Phys. Rev. 76, 1259 (1949).

8. R. Schumacher and N. Vander-Ven, Phys. Rev. (to be published).

9. M. Shimizu and A. Katsuki, J. Phys. Soc. of Japan 19, 614 (1964).

10. C. Townes, C. Herring, and W. Knight, Phys. Rev. 77, 852 (1950).

11. W. Knight, "Electron Paramagnetism and Nuclear Magnetic Resonance in Metals," in Solid State Physics Vol. 2, edited by F. Seitz and D. Turnbull (Academic Press Inc., New York, 1956).

12. T. Rowland, "Nuclear Magnetic Resonance in Metals," in Progress in Materials Science Vol. 9, edited by B. Chalmers (Pergamon Press, New York, 1961).

13. M. Cohen, D. Goodings, and V. Heine, Proc. Phys. Soc. 73, 811 (1959).

14. R. Kubo and Y. Obata, J. Phys. Soc. of Japan 11, 547 (1956).

15. B. McGarvey and H. Gutowsky, J. Chem. Phys. 21, 2114 (1953).

16. G. Benedek and T. Kushida, J. Phys. Chem. Solids 5, 241 (1958).

17. T. Kushida and L. Rimai, Bull. Am. Phys. Soc. 11, 13 (1966); and private communication.

18. T. Kushida and L. Rimai, Phys. Rev. 143, 157 (1966).

19. D. Feldman, Ph.D. thesis, University of California, 1959 (unpublished).

20. R. Snodgrass and L. Bennett, Phys. Rev. 132, 1465 (1963).

21. T. Rowland, J. Phys. Chem. Solids 7, 95 (1958).

22. A. Clogston, V. Jaccarino, and Y. Yafet, Phys. Rev. 134, A650 (1964).

23. N. Bloembergen and T. Rowland, Acta Met. 1, 731 (1953).

24. F. Borsa and R. Barnes, J. Phys. Chem. Solids 25, 1305 (1964).

25. E. Fermi, Z. Physik 60, 320 (1930).

26. D. Pines, "Electron Interaction in Metals," in Solid State Physics Vol. 1, edited by F. Seitz and D. Turnbull (Academic Press Inc., New York, 1955).

27. L. Pauling and E. Wilson Jr., Introduction to Quantum Mechanics (McGraw-Hill, New York, 1935) p. 232.

28. J. Reitz, "Methods of the One-Electron Theory of Solids," in Solid State Physics Vol. 1, edited by F. Seitz and D. Turnbull (Academic Press Inc., New York, 1955).

29. R. Watson and A. Freeman, Phys. Rev. 123, 2027 (1961).

30. V. Jaccarino, Proceedings of the International Conference on Magnetism, Nottingham, 1964 (unpublished).

31. P. Morse and H. Feshback, Methods of Theoretical Physics (McGraw-Hill, New York, 1953) p. 1274.

32. G. Pake, J. Chem. Phys. 16, 327 (1948).

33. T. Muto, S. Kobayasi, M. Watanabe, and H. Kozima, J. Phys. Chem. Solids 23, 1303 (1962).

34. R. Pound and W. Knight, Rev. Sci. Instr. 21, 219 (1950).

35. F. Robinson, J. Sci. Instr. 36, 481 (1959).

36. W. Knight, Rev. Sci. Instr. 32, 95 (1961).

37. R. Brooker, Ph.D. thesis, University of Florida, 1962 (unpublished).

38. P. Haigh, Ph.D. thesis, University of Florida, 1961 (unpublished).

39. S. Hillier, Rev. Sci. Instr. 32, 796 (1961).

40. Instruction Book for Harwood SA10-6-.875PP-200K Intensifier, Harwood Engineering Co., Inc., Walpole, Massachusetts, 1964 (unpublished).

41. G. Benedek and E. Purcell, J. Chem. Phys. 22, 2003 (1954).

42. P. Bridgman, The Physics of High Pressure (G. Bell and Sons, Ltd., London, 1958).

43. The Handbook of Chemistry and Physics, edited by C. Hodgman, R. Weast, and S. Selby (Chemical Rubber Publishing Co., Cleveland, 1955).

44. A. Chapman, P. Rhodes, and E. Seymour, Proc. Phys. Soc. (London) 70B, 345 (1957).

45. L. Piette and H. Weaver, J. Chem. Phys. 28, 735 (1958).

46. R. Corruccini and J. Gniewek, "Thermal Expansion of Technical Solids at Low Temperatures - A Compilation From the Literature," National Bureau of Standards Monograph 29 (U. S. Government Printing Office, Washington, D. C., 1961).

47. R. Wyckoff, Crystal Structures (Interscience Publishers, Inc., New York, 1948).

48. J. Anderson and A. Gold, Phys. Rev. 139, A1459 (1965).

49. R. Prange and L. Kadanoff, Phys. Rev. 134, A566 (1964).

50. Y. Masuda, J. Phys. Soc. of Japan 12, 523 (1957).

BIOGRAPHICAL SKETCH

George Andrew Matzkanin was born on June 30, 1938, in Chicago, Illinois. He attended St. Gall Grammar School and St. Rita High School from which he received his diploma in 1956. He then entered St. Mary's College in Winona, Minnesota from which he was graduated cum laude with a Bachelor of Arts degree in physics in May, 1960.

Upon graduating from St. Mary's, he entered the graduate school at the University of Florida, where he held a teaching assistantship in the Department of Physics from September, 1960, to June, 1962, and a research assistantship from June, 1962, to February, 1966. He received the Master of Science degree with a major in physics in December, 1962, and the Ph.D. degree with a major in physics in April, 1966.

Mr. Matzkanin is married to the former Mary Kathryn Hohn and is the father of a daughter, Karen Terese. He is a member of the American Institute of Physics and the Sigma Xi Honorary Scientific Society.

This dissertation was prepared under the direction of the chairman of the candidate's supervisory committee and has been approved by all members of that committee. It was submitted to the Dean of the College of Arts and Sciences and to the Graduate Council, and was approved as partial fulfillment of the requirements for the degree of Doctor of Philosophy.

April 23, 1966

E. Russell Jones
Dean, College of Arts and Sciences

Dean, Graduate School

Supervisory Committee:

J. A. Scott
Chairman

A. A. Broyles

L. Bailey

F. E. Guerra

R. W. Blaker